COMPASS
www.compassis.com

SeaFEM Theory Manual

SeaFEM

Compass Ingeniería y Sistemas - http://www.compassis.com
Tel:+34 932 181 989 - Fax: +34 933 969 746 - E:info@compassis.com - C/Tuset 8, 7º 2ª, Barcelona 08006 (Spain)

SEAFEM THEORY MANUAL

1. MATHEMATICAL MODEL FOR WAVE PROBLEMS (PART I)

1.1 Glossary

$\boldsymbol{v}_{\varphi}$	Fluid velocity
φ	Velocity potential
ξ	Free surface elevation
$\boldsymbol{v}_{\psi}$	Incident wave induced velocity
ψ	Incident velocity potential
ζ	Incident wave elevation
$\boldsymbol{v}_{\phi}$	Diffraction-radiation wave induced velocity
ϕ	Diffraction-radiation velocity potential
η	Diffraction-radiation wave elevation
P_{fs}	Free surface pressure
P_{ph}^{0}	Hydrostatic pressure at point P.
P_{ph}^{1}	First order hydrostatic pressure variation at point P $\in S_B$.
P_{ph}^{1+2}	Up to second order hydrostatic pressure variation at point P $\in S_B$.
$P_{\psi p}^{1}$	First order pressure at point P induced by INCIDENT wave
$P_{\psi p}^{1+2}$	Up to second order Pressure at point P induced by INCIDENT wave
$P_{\phi p}^{1}$	First order pressure at point P induced by DIF-RAD wave
$P_{\phi p}^{1+2}$	Up to second order Pressure at point P induced by DIF-RAD wave
$\boldsymbol{r}_{p}^{1}$	First order body surface displacement at point P
$\boldsymbol{r}_{p}^{1+2}$	Up to second order body surface displacement at point P
$\mathbf{n}_{\mathrm{p}}$	Body surface normal vector at point P
$\boldsymbol{n}_{p}^{0}$	Initial body surface normal vector at point P
$\boldsymbol{n}_{p}^{1}$	Body surface normal vector after first order movement at point P
$\boldsymbol{v}_{p}^{1}$	First order body velocity over body surface at point P
$\boldsymbol{v}_{p}^{1+2}$	Up to second order body velocity over body surface at point P
$\boldsymbol{X}^{i}$	Up to i-th order displacements

$\boldsymbol{\delta}^i$	Up to i-th order linear displacements
$\boldsymbol{\theta}^i$	Up to i-th order rotational displacements
$\bar{\bar{\boldsymbol{H}}}$	Second order rotation tensor
Ω	Fluid domain
S_B	Instantaneous body boundary
S_B^0	Initial body boundary
S_B^1	Instantaneous body boundary corresponding to first order movements
S_B^{1+2}	Instantaneous body boundary corresponding to up to second order movements
A	Wave amplitude
ω	Wave angular frequency
K	Wave number
α_i	Wave phase delay
H	Water depth

1.2 Governing equations

1.2.1 Flow equation and boundary conditions

Assuming incompressible flow ($\nabla \cdot \mathbf{v} = 0$) and irrotational flow ($\nabla \times \mathbf{v}_\phi = 0 \Rightarrow \mathbf{v}_\phi = \nabla\phi$), then, the flow governing equations are given by:

$\Delta\varphi = 0$	$in\ \Omega$	Potential flow	(1-1)
$\frac{\partial \xi}{\partial t} + \frac{\partial \varphi}{\partial \mathrm{x}}\frac{\partial \xi}{\partial x} + \frac{\partial \varphi}{\partial \mathrm{y}}\frac{\partial \xi}{\partial y} - \frac{\partial \varphi}{\partial \mathrm{z}} = 0$	$on\ z = \zeta$	Free surface kinematic boundary condition	(1-2)
$\frac{\partial \varphi}{\partial \mathrm{t}} + \frac{1}{2}\nabla\varphi \cdot \nabla\varphi + \frac{P_{fs}}{\rho} + g\xi = 0$	$on\ z = \zeta$	Free surface dynamic boundary condition	(1-3)
$\boldsymbol{v}_p \cdot \boldsymbol{n}_p + \boldsymbol{v}_\varphi \cdot \boldsymbol{n}_p = 0$	$on\ S_B$	Body boundary condition	(1-4)
$P_p = -\rho\frac{\partial \varphi}{\partial t} - \frac{1}{2}\rho\nabla\varphi \cdot \nabla\varphi - \rho g z_p$	$in\ \Omega$	Pressure at a point P	(1-5)

1.2.2 Solution approach

Taylor series expansion

Free surface and body boundary condition (BC) will be applied on $z = 0$. Taylor series expansion are carried out to both free surface BCs around $z = 0$ to approximate the BC on $z = \zeta$. Body boundary condition will be applied on S_B^0. Taylor series expansion are carried out around S_B^0 to approximate the BC on S_B.

Perturbed solution

A perturbed solution based on stokes waves approximation is used, where the velocity potential and free surface elevation are perturbed as:

$$\varphi = \epsilon^1\varphi^1 + \epsilon^2\varphi^2 + \epsilon^3\varphi^3 + \cdots \tag{1-6}$$

$$\xi = \epsilon^1\xi^1 + \epsilon^2\xi^2 + \epsilon^3\xi^3 + \cdots \tag{1-7}$$

Body movement solution is also assumed to be a perturbed solution:

$$\boldsymbol{X} = \epsilon^1\boldsymbol{X}^1 + \epsilon^2\boldsymbol{X}^2 + \epsilon^3\boldsymbol{X}^3 \ldots \tag{1-8}$$

$$\boldsymbol{V} = \epsilon^1\boldsymbol{V}^1 + \epsilon^2\boldsymbol{V}^2 + \epsilon^3\boldsymbol{V}^3 \ldots \tag{1-9}$$

Then the translational vector of any point P on the body surface can be perturbed as:

$$\boldsymbol{r}_p = \epsilon^1\boldsymbol{r}_p^1 + \epsilon^2\boldsymbol{r}_p^2 + \epsilon^3\boldsymbol{r}_p^3 \ldots \tag{1-10}$$

where

$$\boldsymbol{X}^i = \left(\delta_x^i, \delta_y^i, \delta_z^i, \theta_x^i, \theta_y^i, \theta_z^i\right) = \left(\boldsymbol{\delta}^i, \boldsymbol{\theta}^i\right) \tag{1-11}$$

$$\boldsymbol{r}_p^1 = \boldsymbol{\delta}^1 + \boldsymbol{\theta}^1 \times \overrightarrow{\boldsymbol{R}^0\boldsymbol{P}^0} \tag{1-12}$$

$$\boldsymbol{r}_p^{1+2} = \boldsymbol{\delta}^{1+2} + \boldsymbol{\theta}^{1+2} \times \overrightarrow{\boldsymbol{R}^0\boldsymbol{P}^0} + \overline{\overline{\boldsymbol{H}}}\overrightarrow{\boldsymbol{R}^0\boldsymbol{P}^0} \tag{1-13}$$

$$\overline{\overline{\boldsymbol{H}}} = \frac{1}{2}\begin{pmatrix} -\left(\theta_y^2 + \theta_z^2\right) & 0 & 0 \\ 2\theta_x\theta_y & -(\theta_x^2 + \theta_z^2) & 0 \\ 2\theta_x\theta_z & 2\theta_y\theta_z & -\left(\theta_x^2 + \theta_y^2\right) \end{pmatrix} \tag{1-14}$$

$$\boldsymbol{V}^i = \left(v_x^i, v_y^i, v_z^i, \omega_x^i, \omega_y^i, \omega_z^i\right) = \left(\boldsymbol{v}^i, \boldsymbol{\omega}^i\right) \tag{1-15}$$

$$\boldsymbol{v}_p^1 = \boldsymbol{v}^1 + \boldsymbol{\omega}^1 \times \overrightarrow{\boldsymbol{R}^0\boldsymbol{P}^0} \tag{1-16}$$

$$\boldsymbol{v}_p^{1+2} = \boldsymbol{v}^{1+2} + \boldsymbol{\omega}^{1+2} \times \overrightarrow{\boldsymbol{R}^0\boldsymbol{P}^0} + \ddot{\bar{\boldsymbol{H}}}\overrightarrow{\boldsymbol{R}^0\boldsymbol{P}^0} \tag{1-17}$$

$$\boldsymbol{n}_p^1 = \boldsymbol{n}_p^0 + \boldsymbol{\theta}^1 \times \boldsymbol{n}_p^0 \tag{1-18}$$

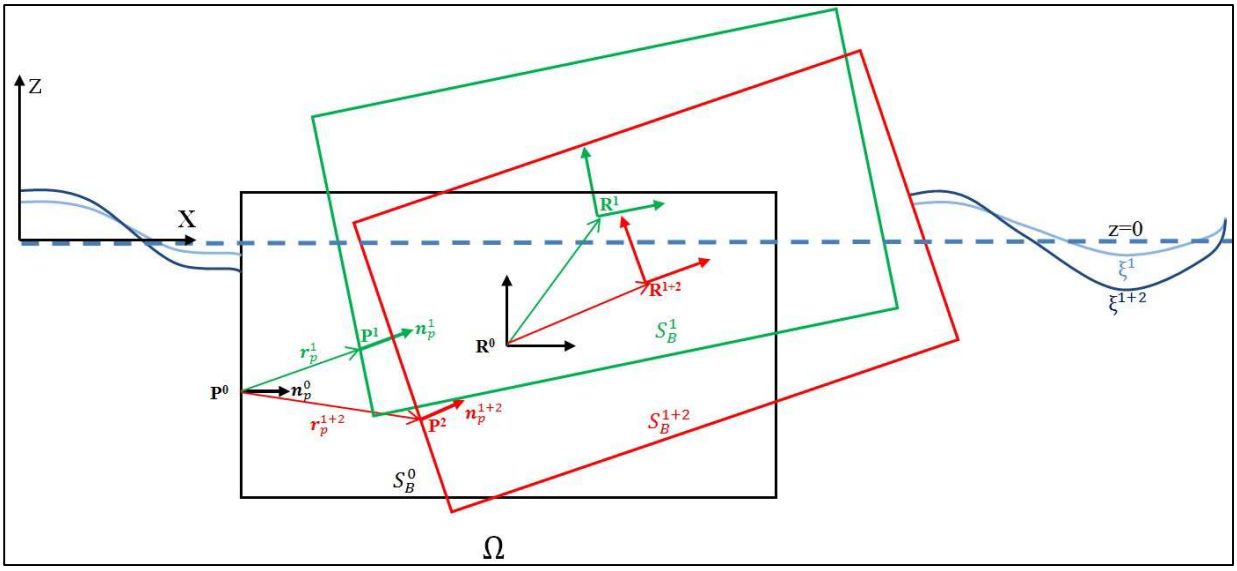

Figure 1: First and second order rigid body movement

1.3 First order approach

1.3.1 First order governing equations

After carrying out the Taylor series expansions, using the perturbed solution, and retaining terms of order ε, the first order governing equations become:

$$\Delta\varphi^1 = 0 \qquad \textbf{in } \boldsymbol{\Omega} \tag{1-19}$$

$$\frac{\partial \xi^1}{\partial t} - \frac{\partial \varphi^1}{\partial z} = 0 \qquad \boldsymbol{in\ z = 0} \tag{1-20}$$

$$\frac{\partial \varphi^1}{\partial t} + \frac{P_{fs}}{\rho} + g\xi^1 = 0 \qquad \boldsymbol{in\ z = 0} \tag{1-21}$$

$$\boldsymbol{v}_p^1 \cdot \boldsymbol{n}_p^0 + \boldsymbol{v}_\varphi^1 \cdot \boldsymbol{n}_p^0 = 0 \qquad \boldsymbol{in\ S_B} \tag{1-22}$$

and the first order pressure at a point P_p^1 on the body surface is

$$P_p^1 = P_H^0 + P_H^1 + P_D^1 \qquad \boldsymbol{in\ S_B} \tag{1-23}$$

where $P_D^1 = -\rho \frac{\partial \varphi^1}{\partial t}$, $P_H^0 = -\rho g z_p$, and $P_H^1 = -\rho g r_{pz}^1$.

1.3.2 First order decomposition solution

The total velocity potential can be decomposed as:

$$\varphi^1 = \psi^1 + \phi^1 \tag{1-24}$$

$$\xi^1 = \zeta^1 + \eta^1 \tag{1-25}$$

where ψ^1 is the incident wave potential, and ϕ^1 is the diffraction-radiation wave potential.

First-order incident wave solution

The incident wave velocity potential ψ^1 fulfils the following equations:

$$\Delta\psi^1 = 0 \qquad \mathbf{in\ \Omega} \tag{1-26}$$

$$\frac{\partial \zeta^1}{\partial t} - \frac{\partial \psi^1}{\partial \mathrm{z}} = 0 \qquad \boldsymbol{on\ z = 0} \tag{1-27}$$

$$\frac{\partial \psi^1}{\partial \mathrm{t}} + g\zeta^1 = 0 \qquad \boldsymbol{on\ z = 0} \tag{1-28}$$

$$\frac{\partial \psi^1}{\partial \mathrm{z}} = 0 \qquad \boldsymbol{on\ z = -H} \tag{1-29}$$

Eqs. (1-26)-(1-28) has an analytical solution, known as the Airy wave solution:

$$\psi^1 = \sum_i \frac{A_i g}{\omega_i} \frac{\cosh\big(|\boldsymbol{k}_i|(H+z)\big)}{\cosh(|\boldsymbol{k}_i|H)} \sin(\boldsymbol{k}_i \boldsymbol{x} - \omega_i t + \alpha_i) \tag{1-30}$$

$$\zeta^1 = \sum_i A_i \cos(\boldsymbol{k}_i \boldsymbol{x} - \omega_i t + \alpha_i) \tag{1-31}$$

where A is the wave amplitude, H is a constant water depth, $\boldsymbol{k} = \frac{2\pi}{L}(\cos(\gamma), \sin(\gamma))$, L is the wave length, γ is the wave propagation direction, $\omega = \frac{2\pi}{T}$, T is the wave period, and α is the wave phase delay. The following dispersion relation holds:

$$\omega_i^2 = g|\boldsymbol{k}_i| \tanh(|\boldsymbol{k}_i|H) \tag{1-32}$$

and the fluid pressure induced by the Airy wave in a point P is given by:

$$P_{p\psi}^1 = \sum_i \rho g A_i \frac{\cosh\big(|\boldsymbol{k}_i|(H+z)\big)}{\cosh(|\boldsymbol{k}_i|H)} \cos\left(\boldsymbol{k}_i \boldsymbol{x} - \omega_i t + \alpha_i\right) \tag{1-33}$$

In the asymptotic case of infinite water depth ($H \to \infty$), the factor $cosh\,(|\boldsymbol{k}|(H+z))/cosh\,(|\boldsymbol{k}|H) \to \exp(|\boldsymbol{k}|z)$.

First-order diffraction-radiation wave problem

The governing equations for the diffraction-radiation velocity potential ϕ^1 is given by:

$$\Delta\phi^1 = 0 \qquad \textbf{in } \boldsymbol{\Omega} \tag{1-34}$$

$$\frac{\partial \eta^1}{\partial t} - \frac{\partial \phi^1}{\partial z} = 0 \qquad \boldsymbol{on\ z = 0} \tag{1-35}$$

$$\frac{\partial \phi^1}{\partial t} + \frac{P_{fs}}{\rho} + g\eta^1 = 0 \qquad \boldsymbol{on\ z = 0} \tag{1-36}$$

$$\boldsymbol{v}_\phi^1 \cdot \boldsymbol{n}_p^0 = -\boldsymbol{v}_p^1 \cdot \boldsymbol{n}_p^0 - \boldsymbol{v}_\psi^1 \cdot \boldsymbol{n}_p^0 \qquad \boldsymbol{on}\ \mathbf{P} \in \mathbf{S_B} \tag{1-37}$$

and the fluid pressure at a point P on the body surface is given by:

$$P_p^1 = P_{ph}^0 + P_{ph}^1 + P_{p\psi}^1 + P_{p\phi}^1 \qquad \boldsymbol{on}\ \mathbf{P} \in \mathbf{S_B} \tag{1-38}$$

where $P_{p\phi}^1 = -\rho \frac{\partial \phi^1}{\partial t}$, $P_{ph}^0 = -\rho g z$, and $P_{ph}^1 = -\rho g r_{pz}^1$.

1.4 Second order approach

1.4.1 Second-order governing equations

After carrying out the Taylor series expansions, using the perturbed solution, and retaining terms up to order ε^2, and considering that $\varphi^{1+2} = \varphi^1 + \varphi^2$, $\xi^{1+2} = \xi^1 + \xi^2$, $P_p^{1+2} = P_p^1 + P_p^2$, $\boldsymbol{X}_B^{1+2} = \boldsymbol{X}_B^1 + \boldsymbol{X}_B^2$, $\boldsymbol{V}_B^{1+2} = \boldsymbol{V}_B^1 + \boldsymbol{V}_B^2$, $\boldsymbol{v}_p^{1+2} = \boldsymbol{v}_p^1 + \boldsymbol{v}_p^2$, $\boldsymbol{v}_\varphi^{1+2} = \boldsymbol{v}_\varphi^1 + \boldsymbol{v}_\varphi^2$, $\boldsymbol{r}_p^{1+2} = \boldsymbol{r}_p^1 + \boldsymbol{r}_p^2$, the governing equations become:

$$\Delta\varphi^{1+2} = 0 \qquad \textbf{in } \boldsymbol{\Omega} \tag{1-39}$$

$$\frac{\partial \xi^{1+2}}{\partial t} - \frac{\partial \varphi^{1+2}}{\partial z} = \xi^1 \frac{\partial}{\partial z}\left(\frac{\partial \varphi^1}{\partial z}\right) - \frac{\partial \xi^1}{\partial x}\frac{\partial \varphi^1}{\partial x} - \frac{\partial \xi^1}{\partial y}\frac{\partial \varphi^1}{\partial y} \qquad \boldsymbol{in\ z = 0} \tag{1-40}$$

$$\frac{\partial \varphi^{1+2}}{\partial t} + \frac{P_{fs}}{\rho} + g\xi^{1+2} = -\xi^1 \frac{\partial}{\partial z}\left(\frac{\partial \varphi^1}{\partial t}\right) - \frac{1}{2}\nabla\varphi^1 \cdot \nabla\varphi^1 \qquad \boldsymbol{in\ z = 0} \tag{1-41}$$

$$\left(\boldsymbol{v}_p^1 + \boldsymbol{v}_\phi^1\right) \cdot \boldsymbol{n}_p^1 + \left(\boldsymbol{v}_p^2 + \boldsymbol{v}_\phi^2\right) \cdot \boldsymbol{n}_p^0 = -(\boldsymbol{r}_p^1 \cdot \nabla \boldsymbol{v}_\phi^1) \cdot \boldsymbol{n}_p^0 \qquad \boldsymbol{in\ S_B^0} \tag{1-42}$$

and the pressure at a point P on the body surface is:

$$P_p^{1+2} = P_H^0 + P_H^{1+2} + P_D^{1+2} \qquad \boldsymbol{in\ S_B^0} \tag{1-43}$$

where $P_H^0 = -\rho g z_p$, and $P_H^{1+2} = -\rho g r_{pz}^{1+2}$, and $P_D^{1+2} = -\rho \frac{\partial \varphi^{1+2}}{\partial t} - \rho \boldsymbol{r}_p^1 \cdot \nabla\left(\frac{\partial \varphi^1}{\partial t}\right) - \rho \frac{1}{2}\nabla\varphi^1 \cdot \nabla\varphi^1$.

1.4.2 Second-order decomposition solution

Second-order incident wave solution

The second-order total velocity potential can be decomposed as:

$$\varphi^2 = \psi^2 + \phi^2 \tag{1-44}$$

$$\xi^2 = \zeta^2 + \eta^2 \tag{1-45}$$

where ψ^2 is the second-order incident wave potential, and ϕ^2 is the second-order diffraction-radiation wave velocity potential. The up to second-order incident wave potential and free surface elevation fulfils the following equations:

$$\Delta\psi^{1+2} = 0 \qquad \textbf{in } \boldsymbol{\Omega} \tag{1-46}$$

$$\frac{\partial\zeta^{1+2}}{\partial t} - \frac{\partial\psi^{1+2}}{\partial \mathrm{z}} = \zeta^1\frac{\partial^2\psi^1}{\partial z^2} - \frac{\partial\zeta^1}{\partial x}\frac{\partial\psi^1}{\partial x} - \frac{\partial\zeta^1}{\partial y}\frac{\partial\psi^1}{\partial y} \qquad \boldsymbol{on\ z = 0} \tag{1-47}$$

$$\frac{\partial\psi^{1+2}}{\partial \mathrm{t}} + g\zeta^{1+2} = -\zeta^1\frac{\partial}{\partial z}\left(\frac{\partial\psi^1}{\partial t}\right) - \frac{1}{2}\nabla\psi^1\cdot\nabla\psi^1 \qquad \boldsymbol{on\ z = 0} \tag{1-48}$$

$$\frac{\partial\psi^{1+2}}{\partial \mathrm{z}} = 0 \qquad \boldsymbol{on\ z = -H} \tag{1-49}$$

The solution to Eqs.(1-46)-(1-49) is as follows:

$$\begin{aligned}\psi^{1+2} = \psi^1 &+ \sum_i B_{ij}^0 \sin\left(2(\boldsymbol{k}_i\boldsymbol{x} - \omega_i t + \alpha_i)\right) \\ &+ \sum_{j>i}\sum_i B_{ij}^+ \cosh\left(\left|\boldsymbol{k}_i + \boldsymbol{k}_j\right|(H+z)\right)\sin\left((\boldsymbol{k}_i\boldsymbol{x} - \omega_i t + \delta_i) + \left(\boldsymbol{k}_j\boldsymbol{x} - \omega_j t + \alpha_j\right)\right) \\ &+ \sum_{j>i}\sum_i B_{ij}^- \cosh\left(\left|\boldsymbol{k}_i - \boldsymbol{k}_j\right|(H+z)\right)\sin\left((\boldsymbol{k}_i\boldsymbol{x} - \omega_i t + \delta_i) - \left(\boldsymbol{k}_j\boldsymbol{x} - \omega_j t + \alpha_j\right)\right)\end{aligned} \tag{1-50}$$

where the coefficients are given in table 1. In the asymptotic case of infinite depth ($H \to \infty$) the coefficients $B_{ij}^0 \to 0$, $D_{ij}^+ \to \infty$, $D_{ij3}^- \to \infty$, $B_{ij}^+ \to 0$, $B_{ij}^- \to 0$. Then, the second order velocity potential becomes null. The wave elevation up to second order is obtained from:

$$\zeta^{1+2} = -\frac{1}{g}\left(\frac{\partial\psi^{1+2}}{\partial \mathrm{t}} + \frac{P}{\rho} + \zeta^1\frac{\partial}{\partial z}\left(\frac{\partial\psi^1}{\partial t}\right) + \frac{1}{2}\nabla\psi^1\cdot\nabla\psi^1 - C^1\right) \tag{1-51}$$

and the fluid pressure induced by the second order wave potential at a point P is:

$$P_{p\psi}^{1+2} = -\rho\left(\frac{\partial\psi^{1+2}}{\partial \mathrm{t}} + \frac{1}{2}\nabla\psi^{1}\cdot\nabla\psi^{1}\right) - \rho\left(\boldsymbol{r}_{p}^{1}\cdot\nabla\left(\frac{\partial\psi^{1}}{\partial t}\right)\right) \tag{1-52}$$

In the asymptotic case of infinite depth ($H \to \infty$) the coefficients $B_{ij}^{0} \to 0$, $D_{ij}^{+} \to \infty$, $D_{ij3}^{-} \to \infty$, $B_{ij}^{+} \to 0$, $B_{ij}^{-} \to 0$. Then, the second order velocity potential becomes null.

Table 1: Stoke´s second-order wave potential coefficients

$B_{ij}^{0} = \frac{3A_i^2 g\lvert\boldsymbol{k}_i\rvert}{8\omega_i}\frac{\cosh\left(2\lvert\boldsymbol{k}_i\rvert(H+z)\right)}{\sinh^3(\lvert\boldsymbol{k}_i\rvert H)\cosh(\lvert\boldsymbol{k}_i\rvert H)}$
$B_{ij}^{+} = \frac{\sum_{k=1}^{3} C_{ijk}^{+}}{D_{ijk}^{+}}$
$B_{ij}^{-} = \frac{\sum_{k=1}^{3} C_{ijk}^{-}}{D_{ijk}^{-}}$
$C_{ij1}^{+} = \frac{A_i A_j}{2g}\omega_i^2(\omega_i + \omega_j)$
$C_{ij1}^{-} = \frac{A_i A_j}{2g}\omega_i^2(\omega_i - \omega_j)$
$C_{ij2}^{+} = \frac{A_i A_j}{4g}(\omega_i\omega_j - g^2\frac{\boldsymbol{k}_i\cdot\boldsymbol{k}_j}{\omega_i\omega_j})(\omega_i + \omega_j)$
$C_{ij2}^{-} = -\frac{A_i A_j}{4g}(\omega_i\omega_j + g^2\frac{\boldsymbol{k}_i\cdot\boldsymbol{k}_j}{\omega_i\omega_j})(\omega_i - \omega_j)$
$C_{ij3}^{+} = -\frac{A_i A_j}{2}\frac{g}{\omega_i}\left(\lvert\boldsymbol{k}_i\rvert^2 + \boldsymbol{k}_i\cdot\boldsymbol{k}_j\right)$
$C_{ij3}^{-} = \frac{A_i A_j}{2}\frac{g}{\omega_i}\left(\lvert\boldsymbol{k}_i\rvert^2 - \boldsymbol{k}_i\cdot\boldsymbol{k}_j\right)$
$D_{ij}^{+} = \lvert\boldsymbol{k}_i + \boldsymbol{k}_j\rvert sinh\left(\lvert\boldsymbol{k}_i + \boldsymbol{k}_j\rvert H\right) - \frac{1}{g}\left(\omega_i + \omega_j\right)^2\cosh\left(\lvert\boldsymbol{k}_i + \boldsymbol{k}_j\rvert H\right)$
$D_{ij3}^{-} = \lvert\boldsymbol{k}_i - \boldsymbol{k}_j\rvert sinh\left(\lvert\boldsymbol{k}_i - \boldsymbol{k}_j\rvert H\right) - \frac{1}{g}\left(\omega_i - \omega_j\right)^2\cosh\left(\lvert\boldsymbol{k}_i + \boldsymbol{k}_j\rvert H\right)$

Second-order diffraction-radiation wave problem

The governing equations for the diffraction-radiation velocity potential up to second-order ϕ^{1+2} is given by:

$$\Delta\phi^{1+2} = 0 \qquad \textbf{in } \Omega \tag{1-53}$$

$$\frac{\partial \eta^{1+2}}{\partial t} - \frac{\partial \phi^{1+2}}{\partial z} = -\frac{\partial \phi^1}{\partial x}\frac{\partial \eta^1}{\partial x} - \frac{\partial \phi^1}{\partial y}\frac{\partial \eta^1}{\partial y} - \frac{\partial \phi^1}{\partial x}\frac{\partial \zeta^1}{\partial x} - \frac{\partial \phi^1}{\partial y}\frac{\partial \zeta^1}{\partial y} - \frac{\partial \psi^1}{\partial x}\frac{\partial \eta^1}{\partial x} - \frac{\partial \psi^1}{\partial y}\frac{\partial \eta^1}{\partial y} \qquad \boldsymbol{in\ z = 0} \tag{1-54}$$

$$\frac{\partial \phi^{1+2}}{\partial t} + \frac{P_{fs}}{\rho} + g\eta^{1+2} = -\eta^1 \frac{\partial}{\partial z}\left(\frac{\partial \phi^1}{\partial t}\right) - \zeta^1 \frac{\partial}{\partial z}\left(\frac{\partial \phi^1}{\partial t}\right) - \eta^1 \frac{\partial}{\partial z}\left(\frac{\partial \psi^1}{\partial t}\right) - \frac{1}{2}\nabla\phi^1 \cdot \nabla\phi^1 - \nabla\psi^1 \cdot \nabla\phi^1 \qquad \boldsymbol{in\ z = 0} \tag{1-55}$$

$$\boldsymbol{v}_\phi^2 \cdot \boldsymbol{n}_p^0 + \boldsymbol{v}_\phi^1 \cdot \boldsymbol{n}_p^1 = -\left(\boldsymbol{v}_p^1 + \boldsymbol{v}_\psi^1\right) \cdot \boldsymbol{n}_p^1 - \left(\boldsymbol{v}_p^2 + \boldsymbol{v}_\psi^2 + \boldsymbol{r}_p^1 \cdot \left(\nabla \boldsymbol{v}_\phi^1 + \nabla \boldsymbol{v}_\psi^1\right)\right) \cdot \boldsymbol{n}_p^0 \qquad \boldsymbol{in}\ \mathbf{P} \in \mathbf{S_B} \tag{1-56}$$

and the fluid pressure at a point P on the body surface is given by:

$$P_p^{1+2} = P_{ph}^0 + P_{ph}^{1+2} + P_{p\psi}^{1+2} + P_{p\phi}^{1+2} \qquad \boldsymbol{in}\ \mathbf{P} \in \mathbf{S_B} \tag{1-57}$$

where $P_{ph}^0 = -\rho g z$, $P_{ph}^{1+2} = -\rho g r_{pz}^{1+2}$ and:

$$P_{p\phi}^{1+2} = -\rho\frac{\partial \phi^{1+2}}{\partial t} - \rho\frac{1}{2}\nabla\phi^1 \cdot \nabla\phi^1 - \rho\nabla\psi^1 \cdot \nabla\phi^1 - \rho r_p^1 \cdot \nabla\left(\frac{\partial \phi^1}{\partial t}\right) \qquad \boldsymbol{in}\ \mathbf{P} \in \mathbf{S_B} \tag{1-58}$$

2. NUMERICAL MODELS (PART I)

2.1 Glossary

ϕ	Diffraction-radiation velocity potential
η	Diffraction-radiation wave elevation
P_{fs}	Free surface pressure
Γ_R	Surface limiting the computational domain in the horizontal directions
R^1	First order source terms in combined FS BC for second order solution
S^1	First order source terms in kinematic BC for second order solution
$\bar{\bar{\mathbf{L}}}$	Laplacian FEM matrix
$\boldsymbol{\phi}$	Vector of diffraction-radiation velocity potential at nodes
$\mathbf{b}^B$	FEM Neumann body boundary condition
$\mathbf{b}^R$	FEM Neumann radiation boundary condition
$\mathbf{b}^{Z_0}$	FEM Neumann free surface boundary condition
$\mathbf{b}^{Z_H}$	FEM Neumann bottom boundary condition
Δt	Time step
$\kappa(\boldsymbol{x})$	Wave absorption coefficient

2.2 Finite element formulation

This section presents the formulation based on the finite element method (FEM) to solve the system of the wave diffraction-radiation problem. This formulation has been developed to be used in conjunction with unstructured meshes. The use of unstructured meshes enhances geometry flexibility and speed ups the initial modelling time.

Let Q_h^* be the finite element space to interpolate functions, constructed in the usual manner. From this space, we can construct the subspace $Q_{h,\phi}$, that incorporates the Dirichlet conditions for the potential ϕ. The space of test functions, denoted by Q_h, is constructed as $Q_{h,\phi}$, but with functions vanishing on the Dirichlet boundary. The weak form of the problem can be written as follows:

Find $[\phi_h] \in Q_{h,\phi}$, by solving the discrete variational problem:

$$\int_{\Omega} \nabla v_h \cdot \nabla \phi_h d\Omega = \int_{\Gamma^B} v_h \cdot \hat{\phi}_n^B d\Gamma + \int_{\Gamma^R} v_h \cdot \hat{\phi}_n^R d\Gamma + \int_{\Gamma^{Z_0}} v_h \cdot \hat{\phi}_n^{Z_0} d\Gamma + \int_{\Gamma^{Z-H}} v_h \cdot \hat{\phi}_n^{Z-H} d\Gamma \quad (2\text{-}1)$$

$\forall v_h \in Q_h$

Where $\hat{\phi}_n^B$, $\hat{\phi}_n^R$, $\hat{\phi}_n^{Z_0}$ and $\hat{\phi}_n^{Z-H}$ are the potential normal gradients corresponding to the Neumann boundary conditions on bodies, radiation boundary, free surface and bottom, respectively. At this point, it is useful to introduce the associated matrix form:

$$\bar{\bar{\mathbf{L}}}\boldsymbol{\phi} = \mathbf{b}^B + \mathbf{b}^R + \mathbf{b}^{Z_0} + \mathbf{b}^{Z-H} \quad (2\text{-}2)$$

where $\bar{\bar{\mathbf{L}}}$ is the standard laplacian matrix, and $\mathbf{b}^B$, $\mathbf{b}^R$, $\mathbf{b}^{Z_0}$, and $\mathbf{b}^{Z-H}$ are the vectors resulting of integrating the corresponding boundary condition terms. Regarding the bottom boundary for the refracted and radiated potential, it is imposed naturally in FEM by $\mathbf{b}^{Z-H} = 0$. A detailed description of the FEM model implemented in SeaFEM can be found in [1]

2.3 Free surface boundary condition

Combining the kinematic and dynamic free surface boundary conditions, the free surface condition reads:

$$\frac{\partial^2 \phi}{\partial t^2} + g\frac{\partial \phi}{\partial z} + \frac{\partial}{\partial t}\left(\frac{P_{fs}}{\rho}\right) + \{Q^1\} = 0, \quad (2\text{-}3)$$

and is implemented as a Neumann boundary condition that fulfils the flux boundary integral:

$$\mathbf{b}^{Z_0} = \bar{\bar{\boldsymbol{M}}}_{\Gamma^{Z_0}}, \quad (2\text{-}4)$$

where $\bar{\bar{\boldsymbol{M}}}_{\Gamma^{Z_0}}$ is the corresponding boundary mass and Q^1 are the transfer terms from the first-order to the second-order problem (see Eqs. (1-54)-(1-55)):

$$Q^1 = \partial_t R^1 - S^1, \quad (2\text{-}5)$$

$$R^1 = \eta^1 \frac{\partial}{\partial z}\left(\frac{\partial \phi^1}{\partial t}\right) + \zeta^1 \frac{\partial}{\partial z}\left(\frac{\partial \phi^1}{\partial t}\right) + \eta^1 \frac{\partial}{\partial z}\left(\frac{\partial \psi^1}{\partial t}\right) + \frac{1}{2}\nabla\phi^1 \cdot \nabla\phi^1 + \nabla\psi^1 \cdot \nabla\phi^1, \quad (2\text{-}6)$$

$$S^1 = \frac{\partial \phi^1}{\partial \mathrm{x}}\frac{\partial \eta^1}{\partial x} + \frac{\partial \phi^1}{\partial \mathrm{y}}\frac{\partial \eta^1}{\partial y} + \frac{\partial \phi^1}{\partial \mathrm{x}}\frac{\partial \zeta^1}{\partial x} + \frac{\partial \phi^1}{\partial \mathrm{y}}\frac{\partial \zeta^1}{\partial y} + \frac{\partial \psi^1}{\partial \mathrm{x}}\frac{\partial \eta^1}{\partial x} + \frac{\partial \psi^1}{\partial \mathrm{y}}\frac{\partial \eta^1}{\partial y} \quad (2\text{-}7)$$

$$-\eta^1\frac{\partial^2\phi^1}{\partial z^2}-\eta^1\frac{\partial^2\psi^1}{\partial z^2}-\zeta^1\frac{\partial^2\phi^1}{\partial z^2},$$

where $(\partial_t R^1)^{n+1} = 25/12(R^1)^{n+1} - 4(R^1)^n + 3(R^1)^{n-1} - 4/3(R^1)^{n-2} + 1/4(R^1)^{n-3}$. Eq. (2-3) is discretized in time using the following numerical scheme:

$$\frac{\phi^{n+1}-2\phi^n+\phi^{n-1}}{\Delta t^2} = -g\phi_z^n - \frac{1}{12\Delta t^2}g(\phi_z^{n+1}+10\phi_z^n+\phi_z^{n-1}) - \frac{P_{fs}^{n+1}-P_{fs}^{n-1}}{\rho 2\Delta t} + \left\{-\frac{1}{12\Delta t^2}((Q^1)^{n+1}+10(Q^1)^n+(Q^1)^{n-1})\right\}, \tag{2-8}$$

where for the specific case where $P_{fs} = 0$, the above scheme becomes a fourth order compact Padé scheme.The free surface elevation is discretized in time using the following fourth order in time numerical scheme:

$$\eta^{n+1} = -\frac{1}{g\Delta t}\left(\frac{25}{12}\phi^{n+1}-4\phi^n+3\phi^{n-1}-\frac{4}{3}\phi^{n-2}+\frac{1}{4}\phi^{n-3}\right) - \frac{P_{fs}^{n+1}}{\rho g}\{-(S^1)^{n+1}\}. \tag{2-9}$$

2.4 Radiation condition and wave absorption

Waves represented by ϕ are born at the bodies and propagate in all directions away from the bodies. These waves have to either be dissipated or to be let go out the domain so they will not come back and interact with the bodies. Because of this, a Sommerfeld radiation condition at the edge of the computational domain is introduced:

$$\partial_t\phi + c\nabla\phi\cdot n_R = 0 \qquad \text{in } \Gamma_R \tag{2-10}$$

where Γ_R is the surface limiting the domain in the horizontal directions, and c is a prescribed wave phase velocity. This radiation condition will let waves moving at velocity c to escape out the domain. The numerical scheme used to implement the radiation condition is

$$(\phi_n^R)^{n+1} = -\frac{\phi^{n-1}-\phi^n}{c\Delta t} \qquad \text{in } \Gamma_R \tag{2-11}$$

However, waves with very different velocities will not be leaving the domain. Hence, wave absorption is also introduced into the dynamic free surface boundary condition by varying the pressure such that:

$$P_{fs}(\boldsymbol{x},t) = \kappa(\boldsymbol{x})\rho\frac{\partial\phi}{\partial z} \tag{2-12}$$

Eq. (2-12) increases pressure when the free surface is moving upwards, while decreases the pressure when the free surface is moving downwards. By doing this, energy is transferred from the waves to the atmosphere and waves are damped. However, the coefficient $\kappa(\boldsymbol{x})$ will be set to zero in the area nearby the bodies so that damping will have no effect on the solution of the wave structure interaction problem.

All the numerical models for the wave diffraction-radiation problem implemented in SeaFEM are based on [1] and [20]

3. HYDRODYNAMIC LOADS ON BODIES (PART I)

3.1 Glossary

φ	Velocity potential
ξ	Free surface elevation
$\boldsymbol{r}_p^1$	First order body surface displacement at point P
$\boldsymbol{r}_p^{1+2}$	Up to second order body surface displacement at point P
$\boldsymbol{n}_p^0$	Initial body surface normal vector at point P
$\boldsymbol{n}_p^1$	Body surface normal vector after first order movement at point P
S_B^0	Initial body boundary
$\boldsymbol{\delta}^1$	First order body displacements
$\boldsymbol{\theta}^1$	First order body rotations
$\overline{\overline{\boldsymbol{K}}}_H$	Hydrostatic restoring matrix
$\forall$	Body displacement
$\boldsymbol{x}_B$	Coordinates of body center of buoyancy
$\boldsymbol{x}_G$	Coordinates of body center of gravity
$\boldsymbol{x}_p$	Coordinates of a point P
$\overrightarrow{\boldsymbol{GP}}$	Vector $\boldsymbol{x}_p - \boldsymbol{x}_G$

3.2 First order loads

Hydrodynamic forces and moments are obtained from direct pressure integration over the body surface. The body gravity center will be used as a reference for body movements and moments acting on it.

$$\boldsymbol{F}^1 = \int_{S_B^0} P_p^1 \boldsymbol{n}_p^0 \, ds = \boldsymbol{F}_H^0 + \boldsymbol{F}_H^1 + \boldsymbol{F}_D^1 \tag{3-1}$$

$$\boldsymbol{M}^1 = \int_{S_B^0} P_p^1 \left(\boldsymbol{x}_G - \boldsymbol{x}_p\right) \times \boldsymbol{n}_p^0 \, ds = \boldsymbol{M}_H^0 + \boldsymbol{M}_H^1 + \boldsymbol{M}_D^1 \tag{3-2}$$

where sub-index H stands for hydrostatic loads and D stands for dynamic loads. The hydrostatic loads are split as follows:

$$\boldsymbol{F}_H^0 = -\int_{S_B^0} \rho g z \boldsymbol{n}_p^0 \, ds = \rho g \forall \tag{3-3}$$

$$\boldsymbol{M}_H^0 = -\int_{S_B^0} \rho g z \overrightarrow{\boldsymbol{G}^0\boldsymbol{P}^0} \times \boldsymbol{n}_p^0 \, ds \tag{3-4}$$

$$\boldsymbol{F}_H^1 = -\int_{S_B^0} \rho g r_{pz}^1 \boldsymbol{n}_p^0 \, ds = \bar{\bar{\boldsymbol{K}}}_H \boldsymbol{\delta}^1 \tag{3-5}$$

$$\boldsymbol{M}_H^1 = -\int_{S_B^0} \rho g r_{pz}^1 \overrightarrow{\boldsymbol{G}^0\boldsymbol{P}^0} \times \boldsymbol{n}_p^0 \, ds = \bar{\bar{\boldsymbol{K}}}_H \boldsymbol{\theta}^1 \tag{3-6}$$

where $\forall$ is the body displacement, and $\bar{\bar{\mathbf{K}}}_H$ is the hydrostatic restoring matrix, which are obtained as follows:

$$\forall = -\int_{S_B^0} z_p n_{pz} ds$$

$$x_B = -\frac{1}{2\forall}\int_{S_B^0} x_p^2 n_{px} ds$$

$$y_B = -\frac{1}{2\forall}\int_{S_B^0} y_p^2 n_{py} ds$$

$$z_B = -\frac{1}{2\forall}\int_{S_B^0} z_p^2 n_{pz} ds$$

$$K_H(3,3) = \rho g \int_{S_B^0} n_{pz} ds \tag{3-7}$$

$$K_H(3,4) = \rho g \int_{S_B^0} (y_p - y_G)\, n_{pz} ds$$

$$K_H(3,5) = -\rho g \int_{S_B^0} (x_p - x_G)\, n_{pz} ds$$

$$K_H(4,4) = \rho g \int_{S_B^0} (y_p - y_G)^2 \, n_{pz} ds + \rho g \forall (z_B - z_G)$$

$$K_H(4,5) = -\rho g \int_{S_B^0} (x_p - x_G)(y_p - y_G)\, n_{pz} ds$$

$$K_H(4,6) = -\rho g \forall (x_B - x_G)$$

$$K_H(5,5) = \rho g \int_{S_B^0} \left(x_p - x_G\right)^2 n_{pz} ds + \rho g \forall (z_B - z_G)$$

$$K_H(5,6) = -\rho g \forall (y_B - y_G)$$

where B stands for the body center of buoyancy, and G for the body center of gravity. The dynamic loads are computed as:

$$\boldsymbol{F}_D^1 = -\int_{S_B^0} \rho \frac{\partial \varphi^1}{\partial t} \boldsymbol{n}_p^0 \, ds \tag{3-8}$$

$$\boldsymbol{M}_D^1 = -\int_{S_B^0} \rho \frac{\partial \varphi^1}{\partial t} \overrightarrow{\boldsymbol{G^0 P^0}} \times \boldsymbol{n}_p^0 \, ds \tag{3-9}$$

3.3 Second order loads

Up to second order loads can be split as:

$$\boldsymbol{F}^{1+2} = \boldsymbol{F}_H^0 + \boldsymbol{F}_H^1 + \boldsymbol{F}_H^2 + \boldsymbol{F}_D^1 + \boldsymbol{F}_D^2 \tag{3-10}$$

$$\boldsymbol{M}^{1+2} = \boldsymbol{M}_H^0 + \boldsymbol{M}_H^1 + \boldsymbol{M}_H^2 + \boldsymbol{M}_D^1 + \boldsymbol{M}_D^2 \tag{3-11}$$

Where the hydrostatic loads are:

$$\begin{aligned} \boldsymbol{F}_H^{1+2} &= -\int_{S_B^0} \rho g \left(z_p + r_{pz}^{1+2}\right) \boldsymbol{n}_p^1 \, ds \\ &= \boldsymbol{F}_H^0 + \boldsymbol{F}_H^1 + \boldsymbol{\theta}^1 \times \boldsymbol{F}_H^1 + \overline{\overline{\boldsymbol{K}}}_H \boldsymbol{\delta}^2 - \int_{S_B^0} \rho g \left(\overline{\overline{\boldsymbol{H}}} \overrightarrow{\boldsymbol{R^0 P^0}}\right)_z \boldsymbol{n}_p^0 \, ds \end{aligned} \tag{3-12}$$

$$\begin{aligned} \boldsymbol{M}_H^{1+2} &= -\int_{S_B^0} \rho g \left(z_p + r_{pz}^{1+2}\right) \overrightarrow{\boldsymbol{G^0 P^0}} \times \boldsymbol{n}_p^1 \, ds \\ &= \boldsymbol{M}_H^0 + \boldsymbol{M}_H^1 + \boldsymbol{\theta}^1 \times \boldsymbol{M}_H^1 + \overline{\overline{\boldsymbol{K}}}_H \boldsymbol{\theta}^2 - \int_{S_B^0} \rho g \left(\overline{\overline{\boldsymbol{H}}} \overrightarrow{\boldsymbol{R^0 P^0}}\right)_z \overrightarrow{\boldsymbol{G^0 P^0}} \times \boldsymbol{n}_p^0 \, ds \end{aligned} \tag{3-13}$$

Then:

$$\boldsymbol{F}_H^2 = \overline{\overline{\boldsymbol{K}}}_H \boldsymbol{\delta}^2 + \boldsymbol{\theta}^1 \times \boldsymbol{F}_H^1 - \int_{S_B^0} \rho g \left(\overline{\overline{\boldsymbol{H}}} \overrightarrow{\boldsymbol{R^0 P^0}}\right)_z \boldsymbol{n}_p^0 \, ds \tag{3-14}$$

$$\boldsymbol{M}_H^2 = \bar{\bar{\boldsymbol{K}}}_H \boldsymbol{\theta}^2 + \boldsymbol{\theta}^1 \times \boldsymbol{M}_H^1 - \int_{S_B^0} \rho g \left(\bar{\bar{\boldsymbol{H}}} \overrightarrow{\boldsymbol{R}^0 \boldsymbol{P}^0} \right)_z \overrightarrow{\boldsymbol{G}^0 \boldsymbol{P}^0} \times \boldsymbol{n}_p^0 \, ds \tag{3-15}$$

On the other hand, dynamic loads up to second order are split in four components:

$$\boldsymbol{F}_D^{1+2} = \boldsymbol{F}_D^1 + \boldsymbol{F}_D^2 = \boldsymbol{F}_D^1 + \boldsymbol{F}_{D1}^2 + \boldsymbol{F}_{D2}^2 + \boldsymbol{F}_{D3}^2 + \boldsymbol{F}_{D4}^2 \tag{3-16}$$

$$\boldsymbol{M}_D^{1+2} = \boldsymbol{M}_D^1 + \boldsymbol{M}_D^2 = \boldsymbol{M}_D^1 + \boldsymbol{M}_{D1}^2 + \boldsymbol{M}_{D2}^2 + \boldsymbol{M}_{D3}^2 + \boldsymbol{M}_{D4}^2 \tag{3-17}$$

where

$$\boldsymbol{F}_{D1}^2 = -\rho \int_{S_B^0} \frac{\partial \varphi^2}{\partial t} \boldsymbol{n}_p^0 \, ds + \boldsymbol{\theta}^1 \times \boldsymbol{F}_D^1 \tag{3-18}$$

$$\boldsymbol{F}_{D2}^2 = -\rho \int_{S_B^0} \left(\boldsymbol{r}_p^1 \cdot \nabla \left(\frac{\partial \varphi^1}{\partial t} \right) \right) \boldsymbol{n}_p^0 \, ds \tag{3-19}$$

$$\boldsymbol{F}_{D3}^2 = -\frac{1}{2} \rho \int_{S_B^0} (\nabla \varphi^1 \cdot \nabla \varphi^1) \boldsymbol{n}_p^0 \, ds \tag{3-20}$$

$$\boldsymbol{F}_{D4}^2 = -\frac{1}{2} \rho g \int_{\Gamma_B^0} \left(\xi^1 - r_{pz}^1 \right)^2 \frac{\boldsymbol{n}_p^0}{\sqrt{1 - {n_{pz}^0}^2}} \, dl \tag{3-21}$$

$$\boldsymbol{M}_{D1}^2 = -\rho \int_{S_b^0} \frac{\partial \varphi^2}{\partial t} \overrightarrow{\boldsymbol{G}^0 \boldsymbol{P}^0} \times \boldsymbol{n}_p^0 \, ds + \boldsymbol{\theta}^1 \times \boldsymbol{M}_D^1 \tag{3-22}$$

$$\boldsymbol{M}_{D2}^2 = -\rho \int_{S_b^0} \left(\boldsymbol{r}_p^1 \cdot \nabla \left(\frac{\partial \varphi^1}{\partial t} \right) \right) \overrightarrow{\boldsymbol{G}^0 \boldsymbol{P}^0} \times \boldsymbol{n}_p^0 \, ds \tag{3-23}$$

$$\boldsymbol{M}_{D3}^2 = -\frac{1}{2} \rho \int_{S_b^0} (\nabla \varphi^1 \cdot \nabla \varphi^1) \overrightarrow{\boldsymbol{G}^0 \boldsymbol{P}^0} \times \boldsymbol{n}_p^0 \, ds \tag{3-24}$$

$$\boldsymbol{M}_{D4}^2 = -\frac{1}{2} \rho g \int_{\Gamma_B^0} \left(\xi^1 - r_{pz}^1 \right)^2 \overrightarrow{\boldsymbol{G}^0 \boldsymbol{P}^0} \times \frac{\boldsymbol{n}_p^0}{\sqrt{1 - {n_{pz}^0}^2}} \, dl \tag{3-25}$$

3.4 Mean drift loads

Being the first and second order responses harmonic and taking time average, the following relations holds when:

$$< F^1 >= 0 \tag{3-26}$$

$$< M^1 >= 0 \tag{3-27}$$

$$< F_H^2 >=< \boldsymbol{\theta}^1 \times \boldsymbol{F}_H^1 > -< \int_{S_B^0} \rho g \left(\overline{\overline{\boldsymbol{H}} \overrightarrow{\boldsymbol{R}^0 \boldsymbol{P}^0}} \right)_z \boldsymbol{n}_p^0 \, ds > \tag{3-28}$$

$$< M_H^2 >=< \boldsymbol{\theta}^1 \times \boldsymbol{M}_H^1 > -< \int_{S_B^0} \rho g \left(\overline{\overline{\boldsymbol{H}} \overrightarrow{\boldsymbol{R}^0 \boldsymbol{P}^0}} \right)_z \overrightarrow{\boldsymbol{G}^0 \boldsymbol{P}^0} \times \boldsymbol{n}_p^0 \, ds > \tag{3-29}$$

$$< F_{D1}^2 >=< \boldsymbol{\theta}^1 \times \boldsymbol{F}_D^1 > \tag{3-30}$$

$$< F_{D2}^2 >= -\rho < \int_{S_B^0} \left(\boldsymbol{r}_p^1 \cdot \nabla \left(\frac{\partial \varphi^1}{\partial t} \right) \right) \boldsymbol{n}_p^0 \, ds > \tag{3-31}$$

$$< F_{D3}^2 >= -\frac{1}{2} \rho < \int_{S_B^0} (\nabla \varphi^1 \cdot \nabla \varphi^1) \boldsymbol{n}_p^0 \, ds > \tag{3-32}$$

$$< F_{D4}^2 >= -\frac{1}{2} \rho g < \int_{\Gamma_B^0} \left(\xi^1 - r_{pz}^1 \right)^2 \frac{\boldsymbol{n}_p^0}{\sqrt{1 - {n_{pz}^0}^2}} dl > \tag{3-33}$$

$$< M_{D1}^2 >=< \boldsymbol{\theta}^1 \times \boldsymbol{M}_D^1 > \tag{3-34}$$

$$< M_{D2}^2 >= -\rho < \int_{S_b^0} \left(\boldsymbol{r}_p^1 \cdot \nabla \left(\frac{\partial \varphi^1}{\partial t} \right) \right) \overrightarrow{\boldsymbol{G}^0 \boldsymbol{P}^0} \times \boldsymbol{n}_p^0 \, ds > \tag{3-35}$$

$$< M_{D3}^2 >= -\frac{1}{2} \rho < \int_{S_b^0} (\nabla \varphi^1 \cdot \nabla \varphi^1) \overrightarrow{\boldsymbol{G}^0 \boldsymbol{P}^0} \times \boldsymbol{n}_p^0 \, ds > \tag{3-36}$$

$$< M_{D4}^2 >= -\frac{1}{2} \rho g < \int_{\Gamma_B^0} \left(\xi^1 - r_{pz}^1 \right)^2 \overrightarrow{\boldsymbol{G}^0 \boldsymbol{P}^0} \times \frac{\boldsymbol{n}_p^0}{\sqrt{1 - {n_{pz}^0}^2}} dl > \tag{3-37}$$

Second order terms depending with non-zero time average depends on first order quantities. Hence, second order drifting loads only depends on the first order problem solution.

4. MATHEMATICAL MODEL FOR WAVE PROBLEMS (PART II)

4.1 Glossary

$\mathbf{T}_b$	Linear velocity of the moving body
$\mathbf{W}_b$	Angular velocity of the moving body
$\mathbf{V}_b$	Moving body total translational velocity
$\mathbf{u}$	Water current velocity
$\boldsymbol{v}_\varphi$	Fluid velocity
φ	Velocity potential
ξ	Free surface elevation
$\boldsymbol{v}_\psi$	Incident wave induced velocity
ψ	Incident velocity potential
ζ	Incident wave elevation
$\boldsymbol{v}_\phi$	Diffraction-radiation wave induced velocity
ϕ	Diffraction-radiation velocity potential
η	Diffraction-radiation wave elevation
P_{fs}	Free surface pressure
P_p	First order pressure at point P induced by DIF-RAD wave
$\boldsymbol{n}_p$	Initial body surface normal vector at point P
$\boldsymbol{v}_p$	First order body velocity over body surface at point P
Ω	Fluid domain
S_B	Initial body boundary
A	Wave amplitude
ω	Wave angular frequency
K	Wave number
δ_i	Wave phase delay
H	Water depth

4.2 Problem statement

In this section the wave problem is coped in the case of body moving across the fluid domain in the presence of waves and water currents. Both, body velocity and water current will be assumed to be much larger than velocities induced by waves and therefore, cannot be assumed to be first order magnitudes.

We consider the first order diffraction-radiation problem of a ship moving on the horizontal plane. The two dimensional movement of the ship is identified by $\mathbf{V}_\mathrm{b}(\mathrm{x}) = \mathbf{T}_\mathrm{b} + \mathbf{W}_\mathrm{b} \times (\mathbf{x} - \mathbf{x}_\mathrm{G})$, where $\mathbf{T}_\mathrm{b}$ and $\mathbf{W}_\mathrm{b}$ are the linear and angular velocity of the moving body.

As before, we assume incompressible and irrotational flow, being φ the velocity potential. The following assumptions are made on the order of magnitude of the velocity components and free surface elevation ξ:

$$
\begin{array}{llll}
|\mathbf{V}_\mathrm{b} \sim O(1)| & |\mathbf{u} \sim O(1)| & \varphi_x \sim O(1) & \boldsymbol{\varphi_y \sim O(1)} \\
\varphi_z \sim O(\epsilon) & \varphi_{\alpha\beta} \sim O(\epsilon) & \xi_x \sim O(\epsilon) & \xi_y \sim O(\epsilon)
\end{array}
\tag{4-1}
$$

Based on the previous assumption, the governing equations for the first order diffraction-radiation wave problem are:

$$\Delta\varphi = 0 \qquad in\ \Omega \qquad \text{Potential flow} \tag{4-2}$$

$$\frac{\partial\varphi}{\partial \mathrm{t}} + \boldsymbol{u} \cdot \nabla_\mathrm{h}\varphi + \frac{1}{2}\nabla_\mathrm{h}\varphi \cdot \nabla_\mathrm{h}\varphi + \frac{P_{fs}}{\rho} + g\xi = 0 \qquad in\ z = 0 \qquad \text{Dynamic boundary condition} \tag{4-3}$$

$$\frac{\partial\xi}{\partial t} + (\boldsymbol{u} + \nabla_\mathrm{h}\varphi) \cdot \nabla_\mathrm{h}\xi - \frac{\partial\varphi}{\partial \mathrm{z}} = 0 \qquad in\ z = 0 \qquad \text{Kinematic boundary condition} \tag{4-4}$$

$$\boldsymbol{v}_p \cdot \boldsymbol{n}_p + \left(\boldsymbol{u} + \boldsymbol{v}_\varphi\right) \cdot \boldsymbol{n}_p = 0 \qquad in\ \mathrm{S}_B \qquad \text{Body boundary condition} \tag{4-5}$$

$$\frac{\partial\varphi}{\partial \mathrm{z}} = 0 \qquad in\ z = -H \qquad \text{Wall boundary condition} \tag{4-6}$$

and the pressure at an arbitrary point of the fluid domain is:

$$P_p = -\rho\left(\frac{\partial\varphi}{\partial t} + \boldsymbol{u} \cdot \nabla_\mathrm{h}\varphi + \frac{1}{2}\nabla\varphi \cdot \nabla\varphi + g z_p\right) \qquad \text{Pressure at a point P} \tag{4-7}$$

4.3 Velocity potential decomposition

In order to solve the governing equations provided in Eqs. (4-2)-(4-6), a velocity potential decomposition is introduced. The total velocity potential can be decomposed as:

$$\varphi = \psi + \phi \tag{4-8}$$

$$\xi = \zeta + \eta \tag{4-9}$$

where ψ and ζ are the incident wave potential and elevation respectively, and ϕ and η are the diffraction-radiation velocity potential and free surface elevation. Then, we can split the governing equations into the following sets of equations:

4.3.1 Set 1: incident waves

$$\Delta\psi = 0 \qquad in\ \Omega \tag{4-10}$$

$$\frac{\partial\psi}{\partial t} + \boldsymbol{u}\cdot\nabla_h\psi + g\zeta = 0 \qquad in\ z = 0 \tag{4-11}$$

$$\frac{\partial\xi}{\partial t} + \boldsymbol{u}\cdot\nabla_h\zeta - \frac{\partial\varphi}{\partial z} = 0 \qquad in\ z = 0 \tag{4-12}$$

$$\frac{\partial\psi}{\partial z} = 0 \qquad in\ z = -H \tag{4-13}$$

This set of equations has an analytical solution (Airy waves):

$$\psi = \sum_i \frac{A_i g}{\omega_i}\frac{\cosh\big(|\boldsymbol{k}_i|(H+z)\big)}{\cosh(|\boldsymbol{k}_i|H)}\sin(\boldsymbol{k}_i(\boldsymbol{x}-\boldsymbol{u}t) - \omega_i t + \delta_i) \tag{4-14}$$

$$\zeta = \sum_i A_i \cos(\boldsymbol{k}_i(\boldsymbol{x}-\boldsymbol{u}t) - \omega_i t + \delta_i) \tag{4-15}$$

4.3.2 Set 2: governing equations of wave diffraction-radiation problem

$$\Delta\phi = 0 \qquad in\ \Omega \qquad (4\text{-}16)$$

$$\frac{\partial\phi}{\partial \mathrm{t}} + \boldsymbol{u}\cdot\nabla_{\mathrm{h}}\phi + \frac{1}{2}\nabla_{\mathrm{h}}\phi\cdot\nabla_{\mathrm{h}}\phi + \nabla_{\mathrm{h}}\psi\cdot\nabla_{\mathrm{h}}\phi + \frac{1}{2}\nabla_{\mathrm{h}}\psi\cdot\nabla_{\mathrm{h}}\psi + \frac{P_{fs}}{\rho} + g\eta = 0 \qquad in\ z = 0 \qquad (4\text{-}17)$$

$$\frac{\partial\eta}{\partial t} + (\boldsymbol{u} + \nabla_{\mathrm{h}}\phi + \nabla_{\mathrm{h}}\psi)\cdot\nabla_{\mathrm{h}}\eta + (\nabla_{\mathrm{h}}\phi + \nabla_{\mathrm{h}}\psi)\cdot\nabla_{\mathrm{h}}\zeta - \frac{\partial\phi}{\partial \mathrm{z}} = 0 \qquad in\ z = 0 \qquad (4\text{-}18)$$

$$\boldsymbol{v}_p\cdot\boldsymbol{n}_p + \left(\boldsymbol{u} + \boldsymbol{v}_\psi + \boldsymbol{v}_\phi\right)\cdot\boldsymbol{n}_p = 0 \qquad in\ \mathrm{S}_B \qquad (4\text{-}19)$$

$$\frac{\partial\phi}{\partial \mathrm{z}} = 0 \qquad in\ z = -H \qquad (4\text{-}20)$$

From first order wave theory, we know that $\psi_\alpha \sim O(\epsilon)$ and $\zeta_\alpha \sim O(\epsilon)$. Then, the terms $\frac{1}{2}\psi\cdot\nabla_{\mathrm{h}}\psi \sim O(\epsilon^2)$, $\nabla_{\mathrm{h}}\psi\cdot\nabla_{\mathrm{h}}\zeta \sim O(\epsilon^2)$, and $\nabla_{\mathrm{h}}\psi\cdot\nabla_{\mathrm{h}}\eta \sim O(\epsilon^2)$. Neglecting these terms in the second set of equations (Eqs. (4-16)-(4-20)), and using the analytical solutions of Airy waves, the governing equations for the first order diffraction-radiation wave problem becomes:

$$\Delta\phi = 0 \qquad in\ \Omega \qquad (4\text{-}21)$$

$$\frac{\partial\phi}{\partial \mathrm{t}} + \boldsymbol{u}\cdot\nabla_{\mathrm{h}}\phi + \frac{1}{2}\nabla_{\mathrm{h}}\phi\cdot\nabla_{\mathrm{h}}\phi + \nabla_{\mathrm{h}}\psi\cdot\nabla_{\mathrm{h}}\phi + \frac{P_{fs}}{\rho} + g\eta = 0 \qquad in\ z = 0 \qquad (4\text{-}22)$$

$$\frac{\partial\eta}{\partial t} + (\boldsymbol{u} + \nabla_{\mathrm{h}}\phi)\cdot\nabla_{\mathrm{h}}\eta + \nabla_{\mathrm{h}}\phi\cdot\nabla_{\mathrm{h}}\zeta - \frac{\partial\phi}{\partial \mathrm{z}} = 0 \qquad in\ z = 0 \qquad (4\text{-}23)$$

$$\nabla_{\mathrm{h}}\phi\cdot\boldsymbol{n}_p = -\left(\boldsymbol{v}_p + \boldsymbol{u} + \boldsymbol{v}_\psi\right)\cdot\boldsymbol{n}_p \qquad in\ \mathrm{S}_B \qquad (4\text{-}24)$$

$$\frac{\partial\phi}{\partial \mathrm{z}} = 0 \qquad in\ z = -H \qquad (4\text{-}25)$$

and the pressure induced by diffracted and radiated waves is:

$$P_p = -\rho\left(\frac{\partial\phi}{\partial t} + (\boldsymbol{u} + \nabla_{\mathrm{h}}\phi + \nabla_{\mathrm{h}}\psi)\cdot\nabla_{\mathrm{h}}\phi\ - \frac{1}{2}\nabla\phi\cdot\nabla\phi\right) \qquad (4\text{-}26)$$

Notice that the terms $\nabla_{\mathrm{h}}\psi\cdot\nabla_{\mathrm{h}}\phi$ and $\nabla_{\mathrm{h}}\phi\cdot\nabla_{\mathrm{h}}\zeta$ accounts for the deviation of the incident Airy waves due to the fact that the incidents waves are transport by a non-uniform flow field. Also, the terms $\nabla_{\mathrm{h}}\phi\cdot\nabla_{\mathrm{h}}\phi$ and $\nabla_{\mathrm{h}}\phi\cdot\nabla_{\mathrm{h}}\eta$ are not subject to any kind of linearization so are, which enables to simulate non-steady base flows.

4.4 Governing equations in a moving frame of reference

Based on the numerical approaches used in this work, it is convenient to solve Eqs. (4-21)-(4-25) in a frame of reference fixed to the moving body rather than on the global frame of reference. Therefore, the aforementioned equations will be solved in a local frame of reference. Figure 2 shows the global and local frame of reference. This frame of reference is assumed to match the global frame at time zero. For an observer sitting in the ship, the flow field around the ship will be $\boldsymbol{U}_b(\boldsymbol{x}) = \boldsymbol{u} - \boldsymbol{V}_b(\boldsymbol{x})$. Therefore, the governing equations in the local frame of reference become:

$$\Delta\phi = 0 \qquad in\ \Omega \tag{4-27}$$

$$\frac{\partial\phi}{\partial \mathrm{t}} + \boldsymbol{U}_b \cdot \nabla_\mathrm{h}\phi + \frac{1}{2}\nabla_\mathrm{h}\phi \cdot \nabla_\mathrm{h}\phi + \nabla_\mathrm{h}\psi \cdot \nabla_\mathrm{h}\phi + \frac{P_{fs}}{\rho} + g\eta = 0 \qquad in\ z = 0 \tag{4-28}$$

$$\frac{\partial\eta}{\partial t} + (\boldsymbol{U}_b + \nabla_\mathrm{h}\phi) \cdot \nabla_\mathrm{h}\eta + \nabla_\mathrm{h}\phi \cdot \nabla_\mathrm{h}\zeta - \frac{\partial\phi}{\partial \mathrm{z}} = 0 \qquad in\ z = 0 \tag{4-29}$$

$$\nabla_\mathrm{h}\phi \cdot \boldsymbol{n}_p = -(\boldsymbol{v}_p + \boldsymbol{u} + \boldsymbol{v}_\psi) \cdot \boldsymbol{n}_p \qquad in\ \mathrm{S}_B \tag{4-30}$$

$$\frac{\partial\phi}{\partial \mathrm{z}} = 0 \qquad in\ z = -H \tag{4-31}$$

and the pressure induced by diffracted and radiated waves is:

$$P_p = -\rho\left(\frac{\partial\phi}{\partial t} + (\boldsymbol{U}_b + \nabla_\mathrm{h}\phi + \nabla_\mathrm{h}\psi) \cdot \nabla_\mathrm{h}\phi\ - \frac{1}{2}\nabla\phi \cdot \nabla\phi\right) \tag{4-32}$$

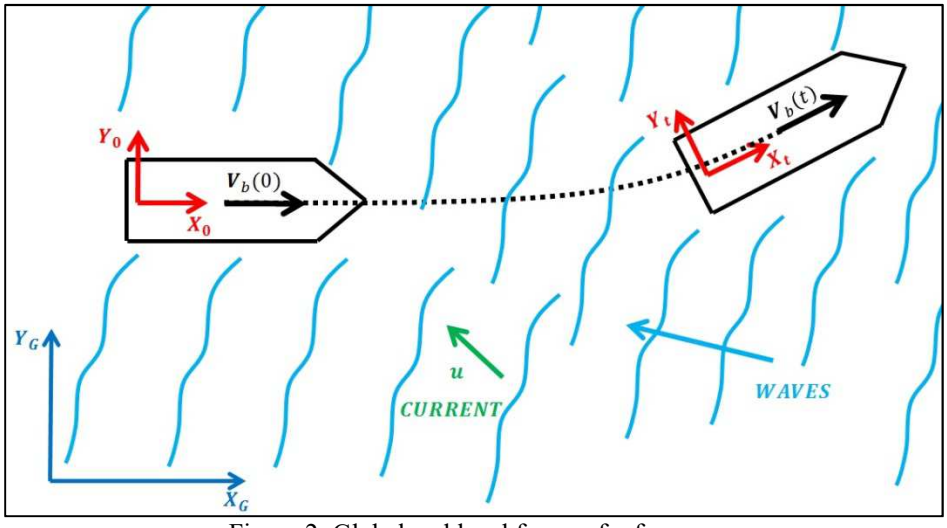

Figure 2: Global and local frame of reference.

where the incident wave potential and incident wave elevation must be transformed to the local frame of reference.

4.5 Flow linearization

The previous governing equations have been obtained under the assumption that $\boldsymbol{v}_{\phi} \sim O(1)$. Then, the free surface boundary conditions can be written as follows:

$$\frac{\partial \phi}{\partial \mathrm{t}} + (\boldsymbol{U}_b + \nabla_{\mathrm{h}}\phi) \cdot \nabla_{\mathrm{h}}\phi - \frac{1}{2}\nabla_{\mathrm{h}}\phi \cdot \nabla_{\mathrm{h}}\phi + \nabla_{\mathrm{h}}\psi \cdot \nabla_{\mathrm{h}}\phi + \frac{P_{fs}}{\rho} + g\eta = 0 \qquad in\ z = 0 \tag{4-33}$$

$$\frac{\partial \eta}{\partial t} + (\boldsymbol{U}_b + \nabla_{\mathrm{h}}\phi) \cdot \nabla_{\mathrm{h}}\eta + \nabla_{\mathrm{h}}\phi \cdot \nabla_{\mathrm{h}}\zeta - \frac{\partial \phi}{\partial \mathrm{z}} = 0 \qquad in\ z = 0 \tag{4-34}$$

where $\mathbf{U}_{\mathrm{b}} + \nabla_{\mathrm{h}}\phi$ represents the convective velocity. Since the convective velocity depends on $\nabla_{\mathrm{h}}\phi$, it must be updated every time step to account for variations of the convective velocity. While retaining this assumption allows for simulating transient flows, linearization of the convective velocity is a reasonable practice in many cases. While SeaFEM is capable of imposing the free surface boundary conditions without linearization at all, two commonly used linearizations are also available.

4.5.1 Neumann-Kelvin linearization

Neumann-Kelvin linearization assumes that $\nabla_{\mathrm{h}}\phi \sim O(\epsilon)$. This assumption is usually made for slender bodies whose perturbation of the flow field is small compared to the convective velocity. Then the convective velocity becomes the apparent velocity between the moving body and the water $\boldsymbol{U}_b(\boldsymbol{x}) = \boldsymbol{u} - \boldsymbol{V}_b(\boldsymbol{x})$. Then the first order free surface boundary conditions become:

$$\frac{\partial \phi}{\partial \mathrm{t}} + \boldsymbol{U}_b \cdot \nabla_{\mathrm{h}}\phi + \frac{P_{fs}}{\rho} + g\eta = 0 \qquad in\ z = 0 \tag{4-35}$$

$$\frac{\partial \eta}{\partial t} + \boldsymbol{U}_b \cdot \nabla_{\mathrm{h}}\eta - \frac{\partial \phi}{\partial \mathrm{z}} = 0 \qquad in\ z = 0 \tag{4-36}$$

and the pressure induced by diffracted and radiated waves is:

$$P_p = -\rho\left(\frac{\partial \phi}{\partial t} + \boldsymbol{U}_b \cdot \nabla_{\mathrm{h}}\phi\right) \tag{4-37}$$

4.5.2 Double body linearization

Double body linearization assumes that $\nabla_{\mathrm{h}}\phi \sim O(1)$ but can be split into two terms: $\nabla_{\mathrm{h}}\phi = \nabla_{\mathrm{h}}\phi^{DB} + \nabla_{\mathrm{h}}\phi^{*}$. $\nabla_{\mathrm{h}}\phi^{DB}$ represents the flow field when the free surface is substituted by a wall (equivalent to a symmetric case using a double body). Then $\nabla_{\mathrm{h}}\phi$ is approximately$\nabla_{\mathrm{h}}\phi^{DB}$, but perturbed by $\nabla_{\mathrm{h}}\phi^{*}$, which means $\nabla_{\mathrm{h}}\phi^{DB} \sim O(1)$ and $\nabla_{\mathrm{h}}\phi^{*} \sim O(\epsilon)$. Then the first order free surface boundary conditions become:

$$\frac{\partial \phi}{\partial \mathrm{t}} + (\boldsymbol{U}_b + \nabla_{\mathrm{h}}\phi^{DB}) \cdot \nabla_{\mathrm{h}}\phi - \frac{1}{2}\nabla_{\mathrm{h}}\phi^{DB}\nabla_{\mathrm{h}}\phi^{DB} + \nabla_{\mathrm{h}}\phi^{DB} \cdot \nabla_{\mathrm{h}}\psi + \frac{P_{fs}}{\rho} + g\eta = 0 \qquad in\ z = 0 \tag{4-38}$$

$$\frac{\partial \eta}{\partial t} + (\boldsymbol{U}_b + \nabla_{\mathrm{h}}\phi^{DB}) \cdot \nabla_{\mathrm{h}}\eta + \nabla_{\mathrm{h}}\phi^{DB} \cdot \nabla_{\mathrm{h}}\zeta - \frac{\partial \phi}{\partial \mathrm{z}} = 0 \qquad in\ z = 0 \tag{4-39}$$

and the pressure induced by diffracted and radiated waves is:

$$P_p = -\rho\left(\frac{\partial \phi}{\partial t} + (\boldsymbol{U}_b + \nabla_{\mathrm{h}}\phi^{DB}) \cdot \nabla_{\mathrm{h}}\phi - \frac{1}{2}\nabla_{\mathrm{h}}\phi^{DB}\nabla_{\mathrm{h}}\phi^{DB} + \nabla_{\mathrm{h}}\phi^{DB} \cdot \nabla_{\mathrm{h}}\psi\right) \tag{4-40}$$

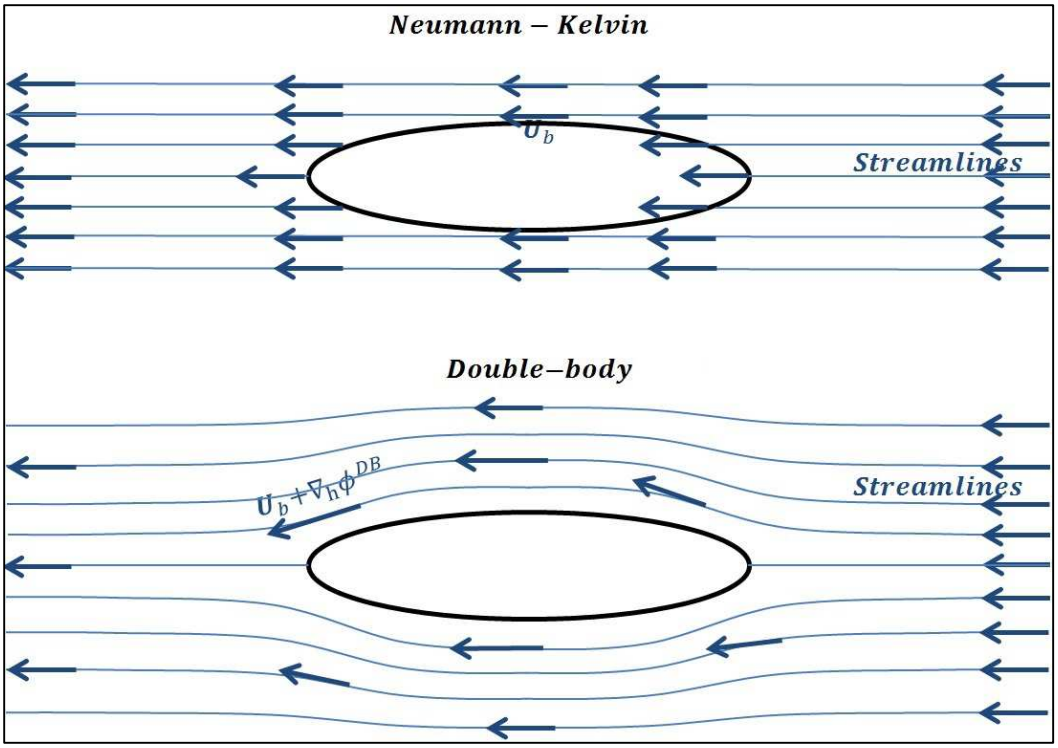

Figure 3: Free surface base flow based on Neumann-Kelvin (up) and double-body (down) linearization concepts.

4.6 Transom stern boundary condition

When considering moving bodies with transom sterns, flow detachment happens at the lower edge of the transom. While potential flow is incapable of predicting this sort of detachment, a transpiration model will be used to enforce it. To do so, the no flux body boundary condition is "not" used, on the contrary, a flux is allowed. The condition to be imposed is that streamlines departing from the detachment edge belong to the free surface. Then, the flux velocity is calculated based assuming that energy at the detachment edge is the same that the energy at the free surface far away downstream, where the free surface remains flat. Using Bernoulli's equation, the flux velocity to be imposed is:

$$\frac{1}{2}\boldsymbol{V}_{ts}^2 - gh = \frac{1}{2}\boldsymbol{V}_{\infty}^2$$
$$U_{ts} = |\boldsymbol{V}_{ts}|\cos(\theta_{ts}) = \sqrt{(\boldsymbol{V}_{\infty}^2 + 2gh)}\cos(\theta_{ts}) \quad (4\text{-}41)$$

Figure 4 explains the transpiration model implemented in SeaFEM.

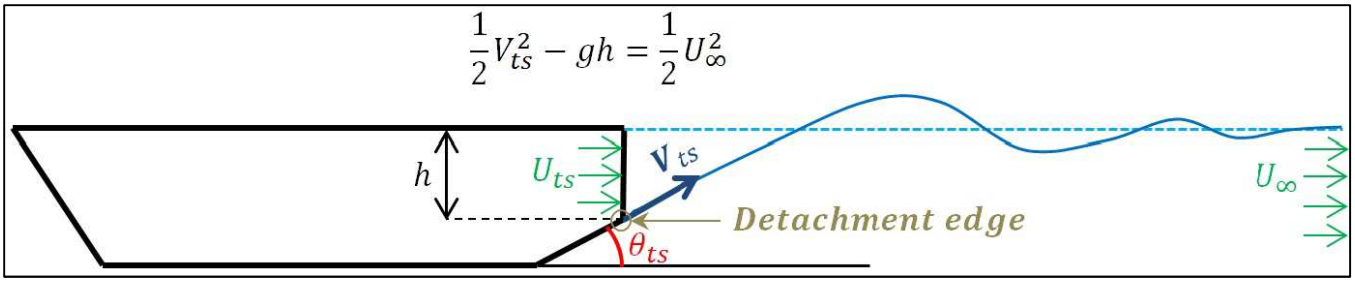

Figure 4: Transpiration model for transom stern Boundary condition with flow detachment.

5. NUMERICAL MODELS (PART II)

5.1 Glossary

ϕ	Diffraction-radiation velocity potential
η	Diffraction-radiation wave elevation
P_{fs}	Free surface pressure
$\boldsymbol{U}$	Free surface convective velocity
$\bar{\bar{\boldsymbol{I}}}$	Identity matrix
$\bar{\bar{\mathbf{W}}}$	Streamline convective matrix
$\bar{\bar{\mathbf{L}}}^{*}$	Modified Laplacian FEM matrix
$\mathbf{b}^{Z_0}$	FEM Dirichlet free surface boundary condition
$\mathbf{b}^{B}$	FEM Neumann body boundary condition
$\mathbf{b}^{Z_H}$	FEM Neumann bottom boundary condition
Δt	Time step
∂_L	Differential operator for first derivative along streamline
θ	Value between 0 and 1.

5.2 Stream line integration

The first order free surface boundary conditions can be written in a general, regardless whether the convective velocity has been linearized or not, as follows

$$\frac{\partial \phi}{\partial \mathrm{t}} + \boldsymbol{U} \cdot \nabla_{\mathrm{h}} \phi + \frac{P_{fs}}{\rho} + g\eta + R = 0 \qquad in\ z = 0 \tag{5-1}$$

$$\frac{\partial \eta}{\partial t} + \boldsymbol{U} \cdot \nabla_{\mathrm{h}} \eta - \frac{\partial \phi}{\partial \mathrm{z}} + \mathrm{S} = 0 \qquad in\ z = 0 \tag{5-2}$$

Where R and S represent some remaining terms. The numerical schemes adopted for solving the kinematic-dynamic free surface boundary conditions are based on Adams-Bashforth-Moulton schemes, using an explicit scheme for the kinematic condition, and implicit one for the dynamic condition. Then ϕ^{n+1} is imposed as a Dirichlet boundary condition. The schemes read as follows:

$$\phi^{n+1} + \Delta t(\boldsymbol{U} \cdot \nabla_h \phi)^{n+1} = \phi^n - \Delta t\left(\frac{1}{\rho} P_{fs}^{n+1} - g\eta^{n+1} - R^{n+1}\right) \qquad in\ z = 0 \tag{5-3}$$

$$\eta^{n+1} = \eta^n - \Delta t(\boldsymbol{U} \cdot \nabla_h \eta)^n + \Delta t(\phi_z^n - S^n) \qquad in\ z = 0 \tag{5-4}$$

where $\boldsymbol{U}$ is the convective velocity. The convective term is obtained by differentiating along streamlines:

$$\begin{aligned}(\boldsymbol{U} \cdot \nabla_h \phi)^{n+1} &= |\boldsymbol{U}|^{n+1} \partial_L \phi^{n+1} \\ (\boldsymbol{U} \cdot \nabla_h \eta)^n &= |\boldsymbol{U}|^n \partial_L \eta^n\end{aligned} \tag{5-5}$$

where ∂_L denotes the derivative along the streamline. This streamline derivative is estimated using a two points upstream and one point downstream differential operator. Figure 5 shows the tracing of the streamline at node C. The left (-1) and forward left (-2) points are the upstream points, while the right (1) point corresponds to the downstream point. The values of the scattered velocity potential ϕ and scattered free surface elevation η at -1, -2 and 1 points are obtained by linear interpolation between the nodes of the edges where they lie on. The stream line differential operator reads as:

$$\begin{aligned}\partial_L \phi_0 &= w_1 \phi_1 + w_0 \phi_0 + w_{-1} \phi_{-1} + w_{-2} \phi_{-2} \\ \partial_L \eta_0 &= w_1 \eta_1 + w_0 \eta_0 + w_{-1} \eta_{-1} + w_{-2} \eta_{-2}\end{aligned} \tag{5-6}$$

where ϕ_1, ϕ_{-1}, ϕ_{-2} are interpolated between (ϕ_{1a}, ϕ_{1b}), (ϕ_{-1a}, ϕ_{-1b}), and (ϕ_{-2a}, ϕ_{-2b}) respectively. In matrix form:

$$\left(\bar{\bar{\boldsymbol{I}}} + \Delta t \bar{\bar{\boldsymbol{W}}}^{\boldsymbol{n+1}}\right)\boldsymbol{\phi}^{n+1} = \bar{\bar{\boldsymbol{I}}}\left(\boldsymbol{\phi}^n - \Delta t\left(\frac{1}{\rho}\boldsymbol{P}_{fs}^{n+1} - g\boldsymbol{\eta}^{n+1} - \boldsymbol{R}^{n+1}\right)\right) \qquad in\ z = 0 \tag{5-7}$$

$$\bar{\bar{\boldsymbol{I}}}\,\boldsymbol{\eta}^{n+1} = \left(\bar{\bar{\boldsymbol{I}}} - \Delta t \bar{\bar{\boldsymbol{W}}}^{\boldsymbol{n}}\right)\boldsymbol{\eta}^n + \Delta t(\boldsymbol{\phi}_z^n - \mathbf{S}^n) \qquad in\ z = 0 \tag{5-8}$$

Where $\bar{\bar{\mathbf{W}}}$ is the streamline convective matrix, and $\bar{\bar{\boldsymbol{I}}}$ is the identity matrix. The stencils are obtained using Taylor series expansion to impose a second order finite difference scheme along the streamline. That is to say, solving the following system of equations:

$$
\begin{aligned}
&w_1 + w_0 + w_{-1} + w_{-2} = 0 \\
&w_1 \Delta x_1 - w_{-1} \Delta x_{-1} - w_{-2} \Delta x_{-2} = 1 \\
&w_1 \frac{\Delta x_1^2}{2} + w_{-1} \frac{\Delta x_{-1}^2}{2} + w_{-2} \frac{\Delta x_{-2}^2}{2} = 0 \\
&w_1 \frac{\Delta x_1^3}{6} - w_{-1} \frac{\Delta x_{-1}^3}{6} - w_{-2} \frac{\Delta x_{-2}^3}{6} = 0
\end{aligned}
\tag{5-9}
$$

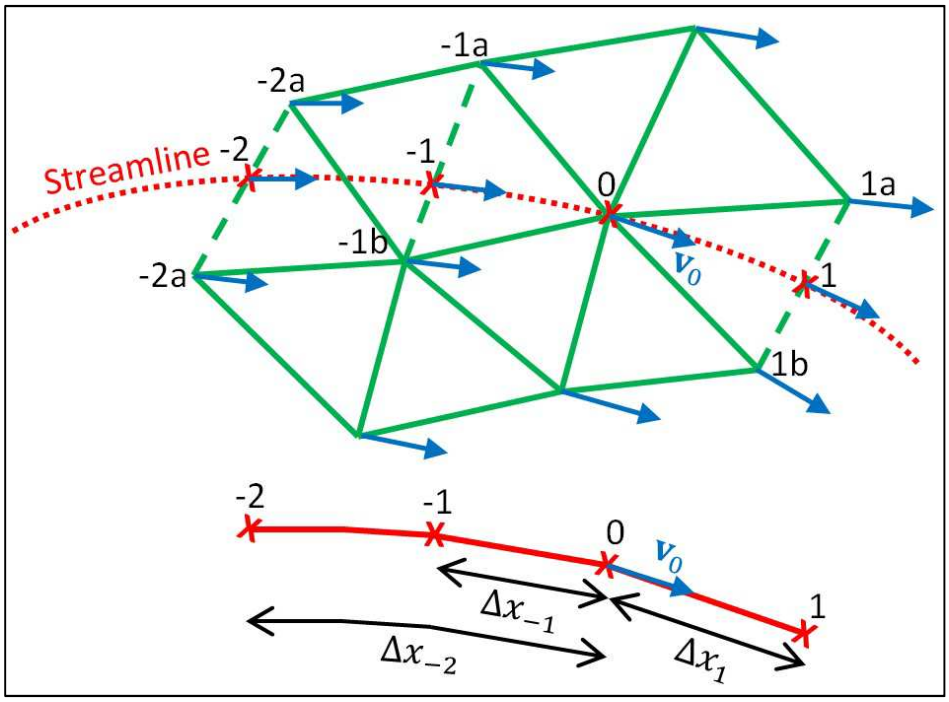

Figure 5: Streamline discretization

The associated matrix form to the finite element formulation for the governing equations is:

$$
\bar{\bar{\mathbf{L}}}^{*} \boldsymbol{\phi} = \mathbf{b}^{Z_0} + \mathbf{b}^{B} + \mathbf{b}^{R} \tag{5-10}
$$

where $\bar{\bar{\mathbf{L}}}^{*}$ is the standard laplacian matrix modified to account for the left hand side of Eq.(5-7), $\mathbf{b}^{Z_0}$ is a vector accounting for the right hand side of Eq. (5-7), and $\mathbf{b}^{B}$ and $\mathbf{b}^{R}$ are the vectors resulting of integrating the corresponding boundary condition terms.

5.3 Streamline Upwind Petrov-Galerkin (SUPG) formulation

Alternatively, a SUPG stabilization scheme is also available in SeaFEM for the integration of the free surface boundary conditions. Both, the dynamic and kinematic boundary conditions can be seen as a convection-reaction equation:

$$\frac{\partial \chi}{\partial \mathrm{t}} + \boldsymbol{U} \cdot \nabla_{\mathrm{h}} \chi + Q = 0 \tag{5-11}$$

Weak formulation:

$$\int_{\Omega} W \left(\frac{\partial \chi}{\partial \mathrm{t}} + \boldsymbol{U} \cdot \nabla_{\mathrm{h}} \chi + Q \right) d\sigma = 0 \tag{5-12}$$

Discrete Galerkin method:

$$\forall i \int_{\Omega} N^i \left(N^j \frac{\partial \chi_j}{\partial \mathrm{t}} + \boldsymbol{U} \cdot \nabla_{\mathrm{h}} N^j \chi_j + N^j Q_j^{n+\theta} \right) d\sigma = 0 \tag{5-13}$$

Time marching scheme:

$$\begin{aligned} &\forall i \int_{\Omega} N^i N^j \frac{{\chi_j}^{n+1} - {\chi_j}^n}{\Delta t} d\sigma + \int_{\Omega} N^i (\mathbf{U}^{n+1} \cdot \nabla_{\mathrm{h}} N^j) \, {\chi_j}^{n+\theta} d\sigma \\ &+ \int_{\Omega} N^i N^j Q_j^{n+\theta} \, d\sigma = 0 \end{aligned} \tag{5-14}$$

SUPG Stabilization:

$$\begin{aligned} &\forall i \sum_e \left\{ \begin{array}{c} \int_{\Omega^e} N^i N^j \frac{{\chi_j}^{n+1} - {\chi_j}^n}{\Delta t} d\sigma + \int_{\Omega^e} N^i \left((\boldsymbol{U^e})^{n+\theta} \cdot \nabla_h N^j \right) {\chi_j}^{n+\theta} d\sigma \\ + \int_{\Omega^e} N^i N^j \left(\frac{P_j^{n+\theta}}{\rho} + g \eta_j^{n+\theta} + R_j^{n+\theta} \right) d\sigma \end{array} \right\} + \\ &\sum_e \frac{h_e (\widehat{\boldsymbol{U}^e})^{n+\theta}}{2 |(\widehat{\boldsymbol{U}^e})^{n+\theta}|} \left\{ \begin{array}{c} \left[\int_{\Omega^e} \nabla_h N^i N^j d\sigma \right] \frac{{\chi_j}^{n+1} - {\chi_j}^n}{\Delta t} + \left[\int_{\Omega^e} \nabla_h N^i \left((\boldsymbol{U}^e)^{n+\alpha} \cdot \nabla_h N^j \right) d\sigma \right] {\chi_j}^{n+\theta} \\ + \left[\int_{\Omega^e} \nabla_h N^i N^j d\sigma \right] Q_j^{n+\theta} \end{array} \right\} = 0 \end{aligned} \tag{5-15}$$

where $\left(\widehat{\mathrm{U}^{\mathrm{e}}}\right)^{\mathrm{n+\theta}}$ is the average convective velocity within the element, and $(\mathrm{U}^{\mathrm{e}})^{\mathrm{n+\alpha}} = \sum_{\mathrm{k_e}} \mathrm{N}^{\mathrm{k_e}} \mathrm{U}_{\mathrm{k_e}}^{\mathrm{n+\alpha}}$. Reordering terms:

$$\begin{aligned}
&\forall i \;\; \sum_{e,i_e,j_e} \left[\int_{\Omega^e} N^{i_e} N^{j_e} \, d\sigma + \frac{h_e (\widehat{\boldsymbol{U}^e})^{n+\theta}}{2\left|(\widehat{\boldsymbol{U}^e})^{n+\theta}\right|} \int_{\Omega^e} \nabla_h N^{i_e} N^{j_e} \, d\sigma \right] \chi_j^{n+1} \\
&- \sum_{e,i_e,j_e} \left[\int_{\Omega^e} N^{i_e} N^{j_e} \, d\sigma + \frac{h_e (\widehat{\boldsymbol{U}^e})^{n+\theta}}{2\left|(\widehat{\boldsymbol{U}^e})^{n+\theta}\right|} \int_{\Omega^e} \nabla_h N^{i_e} N^{j_e} \, d\sigma \right] \chi_j^{n} = \\
&-\Delta t \;\; \sum_{e,i_e,j_e} \left[\int_{\Omega^e} N^{i} \left(N^{k_e} \boldsymbol{U}_{k_e}^{n+\theta} \cdot \nabla_h N^{j_e} \right) d\sigma + \frac{h_e (\widehat{\boldsymbol{U}^e})^{n+\theta}}{2\left|(\widehat{\boldsymbol{U}^e})^{n+\theta}\right|} \int_{\Omega^e} \nabla_h N^{i_e} \left(N^{k_e} \boldsymbol{U}_{k_e}^{n+\theta} \cdot \nabla_h N^{j_e} \right) d\sigma \right] \chi_j^{n+\theta} \\
&-\Delta t \sum_{e,i_e,j_e} \left[\int_{\Omega^e} N^{i_e} N^{j_e} \, d\sigma + \frac{h_e (\widehat{\boldsymbol{U}^e})^{n+\theta}}{2\left|(\widehat{\boldsymbol{U}^e})^{n+\theta}\right|} \int_{\Omega^e} \nabla_h N^{i_e} N^{j_e} \, d\sigma \right] Q_j^{n+\theta}
\end{aligned} \tag{5-16}$$

In matrix form:

$$\begin{aligned}
&\left(\overline{\overline{\boldsymbol{M}}} + \overline{\overline{\boldsymbol{M}}}_{supg}^{n+\theta}\right) \boldsymbol{\chi}^{\mathrm{n+1}} + \boldsymbol{\Delta}\mathrm{t} \left(\overline{\overline{\boldsymbol{C}}}^{n+\theta} + \overline{\overline{\boldsymbol{C}}}_{supg}^{n+\theta}\right) \theta \boldsymbol{\chi}^{\mathrm{n+1}} = \\
&\left(\overline{\overline{\boldsymbol{M}}} + \overline{\overline{\boldsymbol{M}}}_{supg}^{n+1}\right) \boldsymbol{\chi}^{\mathrm{n}} - \boldsymbol{\Delta}\mathrm{t} \left(\overline{\overline{\boldsymbol{C}}}^{n+\theta} + \overline{\overline{\boldsymbol{C}}}_{supg}^{n+\theta}\right) (1-\theta) \boldsymbol{\chi}^{\mathrm{n}} + \left(\overline{\overline{\boldsymbol{M}}} + \overline{\overline{\boldsymbol{M}}}_{supg}^{n+1}\right) \boldsymbol{Q}^{n+\theta}
\end{aligned} \tag{5-17}$$

where:

$$\begin{aligned}
&\overline{\overline{\boldsymbol{M}}} = \sum_{e,i_e,j_e} \int_{\Omega^e} N^{i_e} N^{j_e} \, d\sigma \\
&\overline{\overline{\boldsymbol{M}}}_{supg}^{\mathrm{n+\theta}} = \sum_{e,i_e,j_e} \left[\frac{h_e (\widehat{\boldsymbol{U}^e})^{n+\theta}}{2\left|(\widehat{\boldsymbol{U}^e})^{n+\theta}\right|} \int_{\Omega^e} \nabla_h N^{i_e} N^{j_e} \, d\sigma \right] \\
&\overline{\overline{\boldsymbol{C}}}^{\mathrm{n+\theta}} = \sum_{e,i_e,j_e} \int_{\Omega^e} N^{i} \left(N^{k_e} \boldsymbol{U}_{k_e}^{n+\theta} \cdot \nabla_h N^{j_e} \right) \\
&\overline{\overline{\boldsymbol{C}}}_{supg}^{\mathrm{n+\theta}} = \sum_{e,i_e,j_e} \left[\frac{h_e (\widehat{\boldsymbol{U}^e})^{n+\theta}}{2\left|(\widehat{\boldsymbol{U}^e})^{n+\theta}\right|} \int_{\Omega^e} \nabla_h N^{i_e} \left(N^{k_e} \boldsymbol{U}_{k_e}^{n+\theta} \cdot \nabla_h N^{j_e} \right) d\sigma \right]
\end{aligned} \tag{5-18}$$

Following the same procedure as for the convection-reaction equation, the dynamic boundary condition becomes:

$$\begin{aligned}&\left(\overline{\overline{\boldsymbol{M}}}+\overline{\overline{\boldsymbol{M}}}_{supg}^{n+\theta}\right)\boldsymbol{\phi}^{\mathrm{n+1}}+\Delta\mathrm{t}\left(\overline{\overline{\boldsymbol{C}}}^{n+\theta}+\overline{\overline{\boldsymbol{C}}}_{supg}^{n+\theta}\right)\theta\boldsymbol{\phi}^{\mathrm{n+1}}=\\&\left(\overline{\overline{\boldsymbol{M}}}+\overline{\overline{\boldsymbol{M}}}_{supg}^{n+1}\right)\boldsymbol{\phi}^{\mathrm{n}}-\Delta\mathrm{t}\left(\overline{\overline{\boldsymbol{C}}}^{n+\theta}+\overline{\overline{\boldsymbol{C}}}_{supg}^{n+\theta}\right)(1-\theta)\boldsymbol{\phi}^{\mathrm{n}}-\left(\overline{\overline{\boldsymbol{M}}}+\overline{\overline{\boldsymbol{M}}}_{supg}^{n+1}\right)\left(\frac{1}{\rho}\boldsymbol{P}^{n+\theta}+g\boldsymbol{\eta}^{n+\theta}+\boldsymbol{R}^{n+\theta}\right)\end{aligned} \tag{5-19}$$

And following the same procedure as for the convection-reaction equation, the kinematic boundary condition becomes:

$$\begin{aligned}&\left(\overline{\overline{\boldsymbol{M}}}+\overline{\overline{\boldsymbol{M}}}_{supg}^{n+\theta}\right)\boldsymbol{\eta}^{\mathrm{n+1}}+\Delta\mathrm{t}\left(\overline{\overline{\boldsymbol{C}}}^{n+\theta}+\overline{\overline{\boldsymbol{C}}}_{supg}^{n+\theta}\right)\theta\boldsymbol{\eta}^{\mathrm{n+1}}=\\&\left(\overline{\overline{\boldsymbol{M}}}+\overline{\overline{\boldsymbol{M}}}_{supg}^{n+\theta}\right)\boldsymbol{\eta}^{\mathrm{n}}-\Delta\mathrm{t}\left(\overline{\overline{\boldsymbol{C}}}^{n+\theta}+\overline{\overline{\boldsymbol{C}}}_{supg}^{n+\theta}\right)(1-\theta)\boldsymbol{\eta}^{\mathrm{n}}\\&+\left(\overline{\overline{\boldsymbol{M}}}+\overline{\overline{\boldsymbol{M}}}_{supg}^{n+\theta}\right)\left(\frac{1}{\rho}\boldsymbol{\phi}_{z}^{n+\theta}-\boldsymbol{S}^{n+\theta}\right)\end{aligned} \tag{5-20}$$

The associated matrix form to the finite element formulation for the governing equations is:

$$\overline{\overline{\mathbf{L}}}^{*}\boldsymbol{\phi}=\mathbf{b}^{Z_0}+\mathbf{b}^{B}+\mathbf{b}^{R} \tag{5-21}$$

where $\overline{\overline{\mathbf{L}}}^{*}$ is the standard laplacian matrix modified to account for the left hand side of Eq. (5-19), $\mathbf{b}^{Z_0}$ is a vector accounting for the right hand side of Eq. (5-19), and $\mathbf{b}^{B}$ and $\mathbf{b}^{R}$ are the vectors resulting of integrating the corresponding boundary condition terms.

All the numerical models for the wave diffraction-radiation problem implemented in SeaFEM are based on [1] and [20].

6. HYDRODYNAMIC LOADS ON BODIES (PART II)

6.1 Glossary

φ	Velocity potential
ξ	Free surface elevation
ϕ	Difraction-radiation velocity potential
ϕ^{DB}	Double body diffraction-radiation velocity potential
$\boldsymbol{\delta}^1$	First order body displacements
$\boldsymbol{\theta}^1$	First order body rotations
$\boldsymbol{F}^1$	First order hydrodynamic forces
$\bar{\bar{\boldsymbol{K}}}_H$	Hydrostatic restoring matrix
$\boldsymbol{M}^1$	First order hydrodynamic moments
$\boldsymbol{n}_p^0$	Initial body surface normal vector at point P
P_p^1	First order pressure at point P
$\boldsymbol{r}_p^1$	First order body surface displacement at point P
S_B^0	Initial body boundary
S_{TS}^0	Initial transom stern boundary
$\boldsymbol{U}$	Convective velocity
$\boldsymbol{U_b}$	Body translational velocity
$\boldsymbol{x}_G$	Coordinates of body center of gravity

6.2 First order loads

Hydrodynamic forces and moments are obtained from direct pressure integration over the body surface. The body gravity center will be used as a reference for body movements and moments acting on it.

$$\boldsymbol{F}^1 = \int_{S_B^0} P_p^1 \boldsymbol{n}_p^0 \, ds - \int_{S_{TS}^0} P_p^1 \boldsymbol{n}_p^0 \, ds = \boldsymbol{F}_H^0 + \boldsymbol{F}_H^1 + \boldsymbol{F}_D^1 + \boldsymbol{F}_{TS}^1 \tag{6-1}$$

$$\boldsymbol{M}^1 = \int_{S_B^0} P_p^1 (\boldsymbol{x}_G - \boldsymbol{x}_p) \times \boldsymbol{n}_p^0 \, ds - \int_{S_{TS}^0} P_p^1 (\boldsymbol{x}_G - \boldsymbol{x}_p) \times \boldsymbol{n}_p^0 \, ds = \boldsymbol{M}_H^0 + \boldsymbol{M}_H^1 + \boldsymbol{M}_D^1 + \boldsymbol{M}_{TS}^1 \tag{6-2}$$

where sub-index H stands for hydrostatic loads, D stands for dynamic loads, and TS for transom stern.

6.3 Hydrostatic loads

The hydrostatic loads are split as follows:

$$\boldsymbol{F}_H^0 = -\int_{S_B^0} \rho g z \boldsymbol{n}_p^0 \, ds = \rho g \forall \tag{6-3}$$

$$\boldsymbol{M}_H^0 = -\int_{S_B^0} \rho g z \overrightarrow{\boldsymbol{G}^0\boldsymbol{P}^0} \times \boldsymbol{n}_p^0 \, ds \tag{6-4}$$

$$\boldsymbol{F}_H^1 = -\int_{S_B^0} \rho g r_{pz}^1 \boldsymbol{n}_p^0 \, ds = \overline{\overline{\boldsymbol{K}}}_H \boldsymbol{\delta}^1 \tag{6-5}$$

$$\boldsymbol{M}_H^1 = -\int_{S_B^0} \rho g r_{pz}^1 \overrightarrow{\boldsymbol{G}^0\boldsymbol{P}^0} \times \boldsymbol{n}_p^0 \, ds = \overline{\overline{\boldsymbol{K}}}_H \boldsymbol{\theta}^1 \tag{6-6}$$

where $\forall$ is the body displacement, and $\overline{\overline{\mathbf{K}}}_H$ is the hydrostatic restoring matrix (defined in section 3.2).

6.4 Dynamic loads

The dynamic loads are computed as:

$$\boldsymbol{F}_D^1 = -\int_{S_B^0} \rho \left(\frac{\partial \varphi}{\partial t} + \boldsymbol{U} \cdot \nabla_{\mathrm{h}} \varphi + Q \right) \boldsymbol{n}_p^0 \, ds \tag{6-7}$$

$$\boldsymbol{M}_D^1 = -\int_{S_B^0} \rho \left(\frac{\partial \varphi}{\partial t} + \boldsymbol{U} \cdot \nabla_{\mathrm{h}} \varphi + Q \right) \overrightarrow{\boldsymbol{G}^0\boldsymbol{P}^0} \times \boldsymbol{n}_p^0 \, ds \tag{6-8}$$

where $\boldsymbol{U}$ and Q depends on the flow approximation used (Table 2).

Table 2: values of $\boldsymbol{U}$ and Q (see section 4.5)

Flow type	$\boldsymbol{U}$	Q
Kelvin	$\boldsymbol{U_b}$	0
Double body	$\boldsymbol{U_b} + \nabla_{\mathrm{h}} \phi^{DB}$	$-\frac{1}{2} \nabla_{\mathrm{h}} \phi^{DB} \nabla_{\mathrm{h}} \phi^{DB}$
Non-linear	$\boldsymbol{U_b} + \nabla_{\mathrm{h}} \phi$	$-\frac{1}{2} \nabla_{\mathrm{h}} \phi \cdot \nabla_{\mathrm{h}} \phi$

6.5 Transom stern added resistance

If a transom stern is defined, no hydrodynamic pressure will exist on the transom surface. However, since hydrostatic and dynamic loads are calculated integrating on the initial wet surface of the body, S_B^0

and the transom stern surface is included $S_{TS}^0 \subset S_B^0$, imposing a zero pressure on the transom stern is equivalent to adding the corresponding negative pressure. Then, integrating over S_{TS}^0, the loads obtained can be seen as added resistance due to the lack of hydrostatic and dynamic pressure.

$$\boldsymbol{F}_{TS}^1 = -\int_{S_{TS}^0} P_p^1 \boldsymbol{n}_p^0 \, ds \tag{6-9}$$

$$\boldsymbol{M}_{TS}^1 = -\int_{S_{TS}^0} P_p^1 (\boldsymbol{x}_G - \boldsymbol{x}_p) \times \boldsymbol{n}_p^0 \, ds \tag{6-10}$$

7. BODY DYNAMICS

7.1 Glossary

M	Body mass
$\bar{\bar{\mathbf{I}}}$	Body instantaneous inertia matrix respect to local frame
$\bar{\bar{\boldsymbol{M}}}$	Multibody mass matrix
$\bar{\bar{\boldsymbol{K}}}$	Hydrostatic restoring matrix of the multi-body system
$\mathbf{X}$	Vector containing the six degrees movements of the multi-body system
$\dot{\boldsymbol{X}}$	Vector containing the six degrees velocities of the multi-body system
$\ddot{\boldsymbol{X}}$	Vector containing the six degrees accelerations of the multi-body system
$\mathbf{x}$	Body displacement vector
$\mathbf{r}$	Body rotation vector
$\mathbf{F}$	Vector containing external loads on the multi-body system
$\mathbf{f_i}$	Vector containing external forces on the i^{th} body
$\mathbf{m_i}$	Vector containing external moments on the i^{th} body
α	Alpha modified Bossak-Newmark scheme coefficient
β	Bossak-Newmark beta coefficient
γ	Bossak-Newmark gamma coefficient
$\bar{\bar{\mathbf{A}}}$	Jacobian matrix of body links

7.2 Dynamic equations (small rotations)

Integrating the pressure over the bodies' surface, the resulting forces and moments are obtained. On the other hand, the body dynamics is given by the equation of motion:

$$\bar{\bar{\boldsymbol{M}}}\,\ddot{\boldsymbol{X}} + \bar{\bar{\boldsymbol{K}}}\boldsymbol{X} = \boldsymbol{F} \tag{7-1}$$

SeaFEM uses an implicit alpha modified Bossak-Newmark´s algorithm [2]:

$$(1-\alpha)\mathbf{X}_{tt}^{n+1} + \alpha\mathbf{X}_{tt}^{n} = \bar{\bar{\boldsymbol{M}}}^{-1}\left(\mathbf{F}^{n+1} - \bar{\bar{K}}\mathbf{X}^{n+1}\right) \tag{7-2}$$

$$\mathbf{X}_{t}^{n+1} = \mathbf{X}_{t}^{n} + \Delta t[(1-\gamma)\mathbf{X}_{tt}^{n+1} + \gamma\mathbf{X}_{tt}^{n}] \tag{7-3}$$

$$\mathbf{X}^{n+1} = \mathbf{X}^n + \Delta t \mathbf{X}_t^n + \frac{\Delta t^2}{2}[(1-2\beta)\mathbf{X}_{tt}^{n+1} + 2\beta \mathbf{X}_{tt}^n] \tag{7-4}$$

In the above integration algorithm, α is the parameter defining the numerical damping added in the integration. This damping creates a desirable stabilizing effect in the body dynamics integration. α is usually set to between 0 (no damping) and -0.1. In SeaFEM, γ and β are calculated as γ= 0.5- α and β=0.5γ +0.025α.

7.3 Dynamic equations (large rotations)

In case large rotations are expected, the Euler equations are used to integrate the body dynamics. Each body accelerations are solved respect to a local frame of reference attached to the gravity center of the body, and with axis parallel to the global frame of reference.

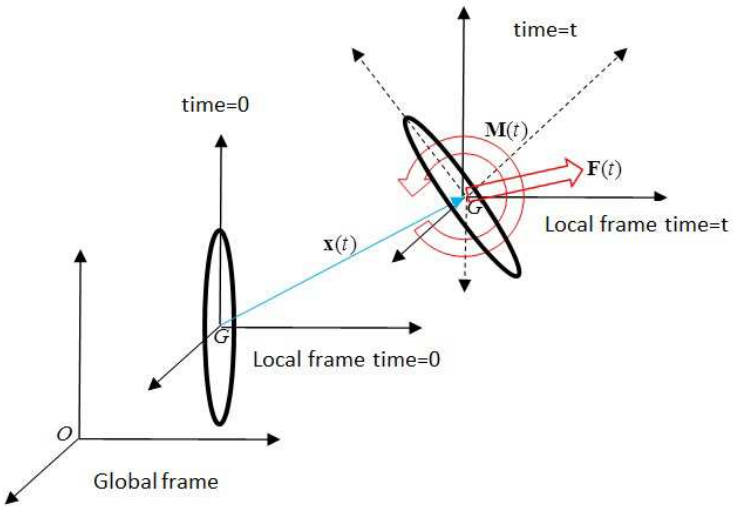

Figure 6: Global and local frame of reference used in SeaFEM

The dynamic equations for each body are the Newton´s and Euler´s equations:

$$\mathrm{M_i}\ddot{\mathbf{x}}_i = \mathbf{f}_\mathrm{i} \tag{7-5}$$

$$\bar{\bar{\mathbf{I}}}_i \ddot{\mathbf{r}}_i = \mathbf{m}_\mathrm{i} - \dot{\boldsymbol{r}}_\mathrm{i} \wedge \left(\bar{\bar{\mathbf{I}}}_\mathrm{i} \cdot \dot{\boldsymbol{r}}_i\right) \tag{7-6}$$

where $\bar{\bar{\mathbf{I}}}_i$ is the instantaneous inertia tensor of body i respect to the local frame. The Euler equations are derived in a rotating reference frame fixed to the body, and therefore, the inertia has to be updated.

It is important to remark that, in equation (7-6), **F** and **M** must be evaluated in the local reference frame.

7.4 Body links

7.4.1 Lagrange multipliers

Let a multibody system be defined by the dynamics equations:

$$\bar{\bar{\mathbf{M}}}\ddot{\mathbf{X}}^t = \mathbf{F}^t \tag{7-7}$$

Let the body-links to be defined by nonlinear equations of the following type:

$$f_{\mathrm{i}}(\mathbf{X}^t) = f_{\mathrm{i}}(X_1^t, X_2^t, \dots, X_{\mathrm{n}}^t) = b_{\mathrm{i}} \tag{7-8}$$

where x_{j}^t is the vector representing the position of all and each body of the multibody system, and b_{i} is a constant value. The latter will be brought into the system dynamics via Lagrange multipliers. To do so, body-links must be linearized. The following linearization is used:

$$f_{\mathrm{i}}\left(X_1^{t,k}, X_2^{t,k}, \dots, X_{\mathrm{n}}^{t,k}\right) + \sum_{\mathrm{j}} \left(\frac{\partial f_{\mathrm{i}}}{\partial x_{\mathrm{j}}}\right)^{t,k} \left(X_{\mathrm{j}}^{t,k+1} - X_{\mathrm{j}}^{t,k}\right) = b_{\mathrm{i}} \tag{7-9}$$

in vector form:

$$(\nabla f_{\mathrm{i}})^{t,k} \cdot \mathbf{X}^{t,k+1} = b_{\mathrm{i}} - f_{\mathrm{i}}(\mathbf{X}^{t,k}) + (\nabla f_{\mathrm{i}})^{t,k} \cdot \mathbf{X}^{t,k} \tag{7-10}$$

where k is the k-th iteration of the iterative resolution of the dynamic system. The previous linearization ensures that as $\|\mathbf{X}^{t,k} - \mathbf{X}^{t,k+1}\| \to 0 \Rightarrow f_{\mathrm{i}}(\mathbf{X}^{t,k+1}) \to b_{\mathrm{i}}$ and the bodylink is fulfilled.
We use an alpha Bossak-Newmark scheme as a temporal integrator scheme for the dynamic equations. Positions $x_{\mathrm{j}}^{t+\Delta t,k+1}$depend linearly on accelerations $\ddot{x}_{\mathrm{j}}^{t+\Delta t,k+1}$as follows:

$$\mathbf{X}^{t,k+1} = \mathbf{X}^{t-\Delta t} + \Delta t\dot{\mathbf{X}}^{t-\Delta t} + \frac{\Delta t^2}{2}\left((1-2\beta)\ddot{\mathbf{X}}^{t-\Delta t} + 2\beta\ddot{\mathbf{X}}^{t,k+1}\right) \tag{7-11}$$

Introducing the Newmark scheme into the linearized bodylink:

$$\begin{aligned}(\nabla f_i)^{t,k} \cdot \left(\mathbf{X}^{t-\Delta t} + \Delta t\dot{\mathbf{X}}^{t-\Delta t} + \Delta t^2\left((0.5-\beta)\ddot{\mathbf{X}}^{t,k+1} + \beta\ddot{\mathbf{X}}^{t-\Delta t}\right)\right) \\ = b_i - f_i(\mathbf{X}^{t,k}) + (\nabla f_i)^{t,k} \cdot \mathbf{X}^{t,k}\end{aligned} \tag{7-12}$$

The previous equation can be written as:

$$\begin{aligned}(\nabla f_i)^{t,k} \cdot \ddot{\mathbf{X}}^{t,k+1} = \frac{1}{\Delta t^2\beta}(b_i - f_i(\mathbf{X}^{t,k}) + (\nabla f_i)^{t,k} \cdot \mathbf{X}^{t,k}) - \\ -(\nabla f_i)^{t,k} \cdot \left(\frac{\mathbf{X}^{t-\Delta t}}{\Delta t^2\beta} + \frac{\dot{\mathbf{X}}^{t-\Delta t}}{\Delta t\beta} + \frac{(0.5-\beta)}{\beta}\ddot{\mathbf{X}}^{t-\Delta t}\right)\end{aligned} \tag{7-13}$$

Or after reordering terms:

$$(\nabla f_i)^{t,k} \cdot \ddot{\mathbf{X}}^{t,k+1} = \frac{1}{\Delta t^2\beta}\left(b_i - f_i(\mathbf{X}^{t,k})\right) + (\nabla f_i)^{t,k} \cdot \ddot{\mathbf{X}}^{t,k} \tag{7-14}$$

The set of linearized bodylinks can be written as:

$$\sum_j \mathrm{a}_{ij}^{t,k}\ddot{X}_j^{t,k+1} = c_i^{t,k} \tag{7-15}$$

where $\bar{\bar{\mathbf{A}}}^{t,k} = \left[\mathrm{a}_{\boldsymbol{ij}}^{t,k}\right]$ is the Jacobian matrix

$$\mathrm{a}_{ij}^{t,k} = \left(\frac{\partial f_i}{\partial x_j}\right)^{t,k} \tag{7-16}$$

and $\boldsymbol{c}^{t,k} = [c_i^{t,k}]$:

$$c_i^{t,k} = \frac{1}{\Delta t^2 \beta}\left[b_i - f_i(\mathbf{X}^{t,k}) + \sum\nolimits_j \mathrm{a}_{ij}^{t,k} X_j^{t,k}\right] - \sum\nolimits_j \mathrm{a}_{ij}^{t,k}\left(\frac{X_j^{t-\Delta t}}{\Delta t^2 \beta} + \frac{\dot{X}_j^{t-\Delta t}}{\Delta t \beta} + \frac{(0.5-\beta)}{\beta}\ddot{X}_j^{t-\Delta t}\right) \tag{7-17}$$

or

$$c_i^{t,k} = \frac{1}{\Delta t^2 \beta}[b_i - f_i(\mathbf{x}^{t,k})] + \sum\nolimits_j \mathrm{a}_{ij}^{t,k} \ddot{X}_j^{t,k} \tag{7-18}$$

Then, the imposition of nonlinear bodylinks via Lagrange multipliers can be carried out as follows:

$$\begin{bmatrix} \bar{\bar{\mathbf{M}}} & \left(\bar{\bar{\mathbf{A}}}^T\right)^{t,k} \\ \bar{\bar{\mathbf{A}}}^{t,k} & 0 \end{bmatrix} \begin{bmatrix} \ddot{\mathbf{x}}^{t,k+1} \\ \boldsymbol{\lambda}^{t,k+1} \end{bmatrix} = \begin{bmatrix} \mathbf{F}^{t,k} \\ \boldsymbol{c}^{t,k} \end{bmatrix} \tag{7-19}$$

Finally, reaction forces are obtained from:

$$\mathbf{R}^{t,k} = -\left(\bar{\bar{\boldsymbol{A}}}^T\right)^{t,k} \boldsymbol{\lambda}^{t,k} \tag{7-20}$$

and since matrix contains the instantaneous normal direction to the trajectory imposed by the body-links, reaction forces act perpendicular to the imposed trajectories.

7.4.2 Body links with Alpha Bossak-Newmark integration

The alpha Bossak-Newmark scheme uses the following scheme to obtain the acceleration at time t:

$$(1-\alpha)\bar{\bar{\mathbf{M}}}\ddot{\mathbf{X}}^t + \alpha\bar{\bar{\mathbf{M}}}\ddot{\mathbf{X}}^{t-\Delta t} = \mathbf{F}^t + \mathbf{R}^t \tag{7-21}$$

where $\mathbf{R}^t = -\bar{\bar{\mathbf{A}}}^T \boldsymbol{\lambda}^t$ are the reaction forces due to bodylinks. Then:

$$\bar{\bar{\mathbf{M}}}(1-\alpha)\ddot{\mathbf{x}}^t + \bar{\bar{\mathbf{A}}}^T \boldsymbol{\lambda}^t = \mathbf{F}^t - \alpha\mathbf{M}\ddot{\mathbf{x}}^{t-\Delta t} \tag{7-22}$$

Introducing the body link constraints $\mathbf{A}\ddot{\mathbf{x}}^t = \boldsymbol{c}^t$, the multibody dynamic system reads as:

$$\begin{bmatrix} \bar{\bar{\mathbf{M}}} & \bar{\bar{\mathbf{A}}}^T \\ \bar{\bar{\mathbf{A}}} & \mathbf{0} \end{bmatrix} \begin{bmatrix} (1-\alpha)\ddot{\mathbf{x}}^t \\ \boldsymbol{\lambda}^t \end{bmatrix} = \begin{bmatrix} \mathbf{F}^t - \alpha\bar{\bar{\mathbf{M}}}\ddot{\mathbf{x}}^{t-\Delta t} \\ (1-\alpha)\boldsymbol{c}^t \end{bmatrix} \tag{7-23}$$

7.5 Body dynamics iterative solver

The dynamic solver is implemented in SeaFEM by means of three nested loops. A relaxation algorithm based on the Aitken´s method [6] is used to speed up convergence within each loop.

7.5.1 Time marching loop

The time marching loop is the outer loop marching in time. Information from the previous time step is used as initial guests of the iterative procedure.

7.5.2 Solver loop

The solver loop is where the hydrodynamic loads are calculated. In each iteration within this loop, the linear system corresponding to the wave diffraction-radiation problem is to be solved. Iterations is carried out until convergence of hydrodynamic loads along with body kinematics is reached.
Should non-linear mooring lines be defined, stiffness linearization will be carried out for each iteration, and the updated stiffness matrix will be passed on to the body dynamics loop.

7.5.3 Body dynamics loop

The body dynamics loop is the inner loop. Within this loop, wave diffraction and radiation loads remain unchanged, hydrostatic forces are updated based on body position, and the rest of loads will be updated in each iteration.

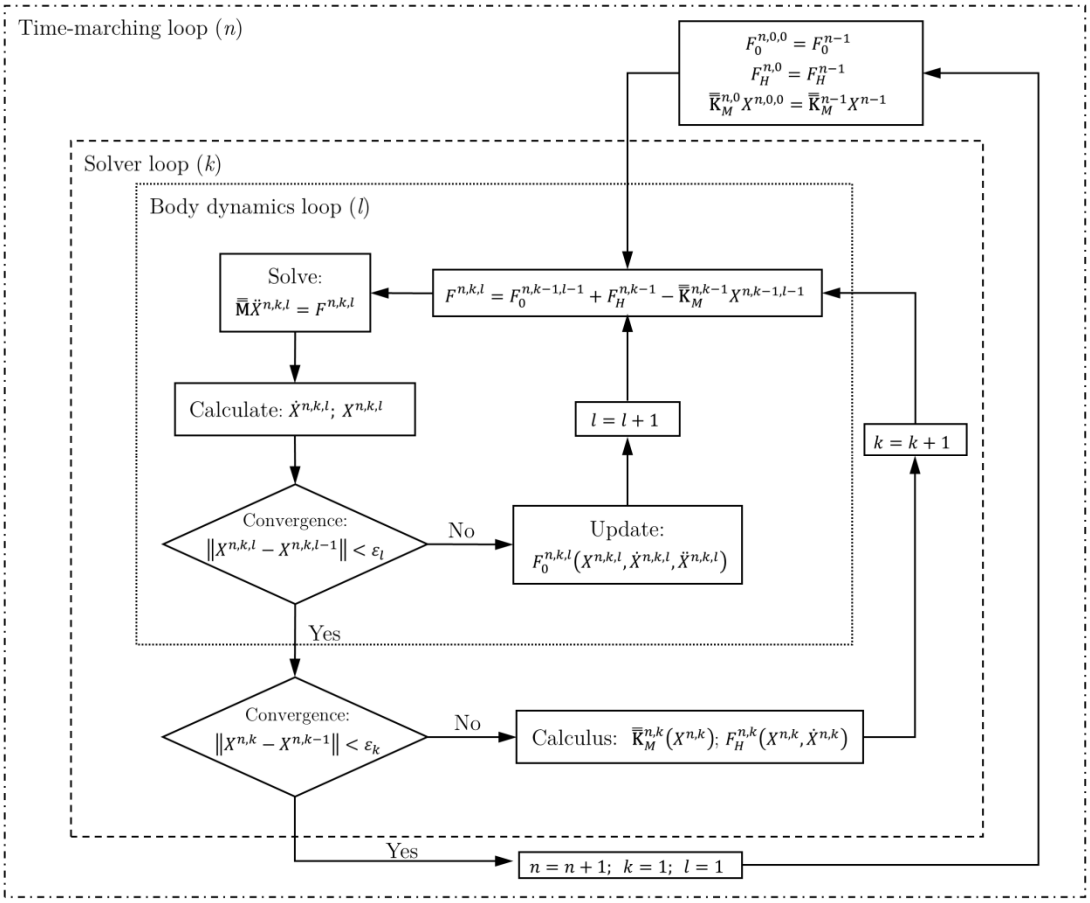

Figure 7: Scheme of the dynamic integration solver of SeaFEM

8. STATISTICAL DESCRIPTION OF WAVES

8.1 Glossary

$S(\omega,\alpha)$	Two dimensional wave energy density distribution
A	Wave amplitude
T	Wave period
ω	Wave angular frequency
k	Wave number
α	Wave direction
η	Wave elevation
δ	Wave phase
H	Water depth
H_S	Significant wave height
T_m	Mean wave period
T_p	is the peak wave period
m_0	Zero order moment of wave energy distribution
m_1	First order moment of wave energy distribution

8.2 Spectrum discretization

Let be $S(\omega,\alpha)$ an energy density spectrum describing a sea state in terms of the wave frequency and direction of propagation. The discretization procedure to obtain a stationary and ergodic realization based on monochromatic waves is as follows:

Let be $\omega_{\min}$ the minimum frequency to be considered, ω_{max} the maximum frequency to be considered, $\alpha_{\min}$ the lower direction of propagation to be considered, α_{max} the larger direction of propagation to be considered, N^w the number of wave frequencies, and N^α the number of wave directions to be considered. Then, the frequency and direction discretization sizes are given by:

$$\Delta\omega = \frac{(\omega_{max} - \omega_{min})}{N^w} \tag{8-1}$$

$$\Delta\alpha = \frac{(\alpha_{max} - \alpha_{min})}{(N^{\alpha} - 1)}$$

then, the wave elevation is given by:

$$\eta = \sum_{i=1}^{N^w} \sum_{j=1}^{N^\alpha} A_{ij} \cos\left(k_{ij} cos(\alpha_j) x + k_{ij} sin(\alpha_j) - \Omega_{ij} t + \delta_{ij}\right) \tag{8-2}$$

where Ω_{ij} is the wave angular velocity and a random variable with uniform distribution in within $[\omega_i - \frac{\Delta\omega}{2}, \omega_i + \frac{\Delta\omega}{2}]$, $\omega_i = \omega_{min} + (i - 1/2)\Delta\omega$, $\alpha_j = \alpha_{min} + (j - 1)\Delta\alpha$, δ_{ij} is a random variable with uniform distribution in $[0, 2\pi]$, t represents time, and x, y are the horizontal Cartesian coordinates. The wave number is obtained from the dispersion relationship:

$$\Omega^2{}_{ij} = g k_{ij} \tanh\left(k_{ij} H\right) \tag{8-3}$$

and the wave amplitude is calculated from the wave energy distribution as:

$$\mathrm{A}_{ij} = \sqrt{2\Delta\omega\Delta\alpha\, S(\omega_i, \alpha_j)} \frac{\frac{1}{16} H_S^2}{\sum_{l,m} \sqrt{2\Delta\omega\Delta\alpha\, S(\omega_l, \alpha_m)}} \tag{8-4}$$

where $H_S = 4\sqrt{m_0}$ is the significant wave height, and $m_0 = \int_0^{\infty} \int_{-\pi}^{\pi} S(\omega, \alpha) d\omega d\alpha$ is zero order moment of the spectrum wave energy.

8.3 Convergence

Convergence of the discretized spectrum will happen as $\omega_{\min} \to 0$, $\omega_{\max} \to \infty$, $\Delta\omega \to 0$, $\alpha_{\min} \to 0$, $\alpha_{\max} \to 2\pi$, and $\Delta\alpha \to 0$. The rate of convergence with $\Delta\omega$ and $\Delta\alpha$ is that of the rectangle rule of numerical integration.

8.4 Spectral moments

8.4.1 Zero order moment

The spectral energy of a wave spectrum is given by: $m_0 = \int_0^\infty \int_{-\pi}^{\pi} S(\omega,\alpha)\, d\omega d\alpha = \frac{1}{16}\rho g\, H_S^2$. Then, the discrete spectrum is scaled such that the spectral moment m_0 is conserved. Therefore:

$$\sum_{i,j} \frac{1}{2} A_{ij}^2 = \frac{1}{16} H_S^2 \tag{8-5}$$

8.4.2 First order moment

The first order moment of the discrete spectrum is:

$$m_1^* = \sum_{i,j} S(\omega_i,\alpha_j)\Omega_{i,j}\Delta\omega\Delta\alpha = \sum_{i,j} S(\omega_i,\alpha_j)\omega_{i,j}\Delta\omega\Delta\alpha + \sum_{i,j} S(\omega_i,\alpha_j)\epsilon_{i,j}\Delta\omega\Delta\alpha \tag{8-6}$$

where ε_{ij} is uniform distributed between $[-\Delta\omega/2, \Delta\omega/2]$, $\sum_{i,j} S(\omega_i,\alpha_j)\omega_{i,j}\Delta\omega\Delta\alpha$ is a deterministic component of the first moment, and $\sum_{i,j} S(\omega_i,\alpha_j)\epsilon_{i,j}\Delta\omega\Delta\alpha$ is a random component. Assuming that $\omega_{\max} \to \infty$, $\omega_{\min} = 0$, $\alpha_{\min} = 0$, $\alpha_{\max} = 2\pi$, the deterministic component converges to:

$$\lim_{\substack{\Delta\omega\to 0 \\ \Delta\alpha\to 0}} \sum_{i,j} S(\omega_i,\alpha_j)\omega_{i,j}\Delta\omega\Delta\alpha = \int_0^\infty \int_{-\pi}^{\pi} \omega S(\omega,\alpha)\, d\omega d\alpha \tag{8-7}$$

On the other hand, for large values of N^ω, the probabilistic component is a random variable with normal distribution. The mean μ and variance σ^2 of this distribution are:

$$\mu = \sum_{i,j} S(\omega_i,\alpha_j)\Delta\omega\Delta\alpha \int_{-\Delta\omega/2}^{\Delta\omega/2} \omega \frac{1}{\Delta\omega} d\omega \tag{8-8}$$

$$\sigma^2 = \sum_{i,j} S(\omega_i, \alpha_j)\Delta\omega\Delta\alpha \int_{-\Delta\omega/2}^{\Delta\omega/2} \omega^2 \frac{1}{\Delta\omega} d\omega = \sum_{i,j} S(\omega_i, \alpha_j)\Delta\omega\Delta\alpha \frac{\Delta\omega^2}{12} \tag{8-9}$$

The probabilistic component converges to a random variable with zero mean and zero variance.

8.5 Wave spectrums

8.5.1 Pearson Moskowitz

This is probably the simplest idealized spectrum, obtained by assuming a fully developed sea state, generated by wind blowing steadily for a long time over a large area [3]. The resulting spectrum was [4]:

$$S(T) = H_s^2 T_m (0.11/2\pi)(T_m/T)^{-5} e^{-0.44(Tm/T)^{-4}} \tag{8-10}$$

where $T_m = 2\pi m_0/m_1$, with m_0 and m_1 the zero and first moments of the wave spectrum.

8.5.2 Jonswap

The JONSWAP spectrum was established during a joint research project, the "JOint North Sea WAve Project" [5]. This is a peak-enhanced Pierson-Moskowitz spectrum given on the form:

$$S(T) = \left(\frac{5}{32\pi} H_s^2 \frac{\mathrm{T}^5}{\mathrm{T_p^4}}\right) \cdot \varepsilon^{\gamma} \cdot \mathrm{e}^{-1.25\left(\mathrm{T_p}/\mathrm{T}\right)^{-4}} \cdot \left(1 - 0.287\log(\epsilon)\right)$$
$$\gamma = \mathrm{e}^{-\left[(0.159\omega \mathrm{T_p} - 1)/(\sigma\sqrt{2})\right]^2} \tag{8-11}$$

where $\omega = 2\pi/T$, $\sigma = 0.07$ for $\omega \leq 6.28/T_p$, $\sigma = 0.09$ for $\omega > 6.28/T_p$, T is the wave period; H_s is the significant wave height, $\mathrm{T_p}$ is the peak wave period and ϵ is the peakedness parameter.

An alternative definition of the JONSWAP spectrum is given by [4]:

$$S(\omega) = \left(\frac{155 H_s^2}{\mathrm{T_m^4}\omega^5}\right) \cdot 3.3^{\gamma} \cdot \mathrm{e}^{-944\mathrm{T_m^{-4}}\,\omega^{-4}} \tag{8-12}$$

$\gamma = \mathrm{e}^{-\left[(0.191\omega \mathrm{T}_{\mathrm{m}}^{-1})/(\sigma\sqrt{2})\right]^2}$

where $\sigma = 0.07$ for $\omega \leq 5.24/T_m$, $\sigma = 0.09$ for $\omega > 5.24/T_m$, $T_m = 2\pi m_0/m_1$.

8.5.3 White noise

The white noise spectrum corresponds to a uniform energy distribution within a wave frequency interval, having zero energy outside the prescribed interval. This type of spectrum is used in SeaFEM to carry out Response amplitude operators (RAOs) analyses (see section 11).

9. MOORING

9.1 Glossary

Elastic catenary formulation

x, z	Horizontal and vertical positions measured from the lower cable point
s	Catenary arc length
T_o	Horizontal component of the cable tension
ω	Catenary weight per unit length in water (i.e. minus buoyancy)
T_v	Vertical component of the cable tension
L	Total length of the catenary
H_F	Horizontal component of the effective tension in the mooring line at the fairlead
V_F	Vertical component of the effective tension in the mooring line at the fairlead
H_F	Horizontal component of the effective tension in the mooring line at the anchor
V_F	Vertical component of the effective tension in the mooring line at the anchor
E	Young's modulus of the mooring line
A	Cross section area of the mooring segment
x_F, z_F	Horizontal and vertical coordinates of the fairlead point relative to the anchor
C_B	Static friction coefficient
L_B	Length of the cable's portion resting at the seabed

Dynamic cables formulation

$\mathbf{x}$	Vector of nodal translational degrees of freedom
$\mathbf{F}$	Vector of external loads
$\overline{\overline{\mathbf{M}}}$	Inertia matrix
$\overline{\overline{\mathbf{M}}}_{\mathrm{A}}$	Added mass matrix
$\mathbf{P}^0$	Pretension vector in the initial configuration
$\mathbf{R}$	Vector of nodal internal forces of the cable
$\overline{\overline{\boldsymbol{C}}}$	Damping matrix
$\overline{\overline{\mathbf{K}}}$	Material stiffness matrix
$\overline{\overline{\mathbf{K}}}_{\mathrm{G}}$	Geometric stiffness matrix
$\overline{\overline{\mathbf{k}}}^{\mathrm{e}}$	Elemental material stiffness matrix

$\bar{\bar{\mathbf{k}}}_G^e$	Elemental geometric stiffness matrix
e	Truss element strain
V^e	Element volume
s	Axial stress
E	Axial elastic modulus
$\bar{\bar{\mathbf{m}}}^e$	Elemental inertia matrix
$\bar{\bar{\mathbf{m}}}_a^{\ e}$	Elemental added mass matrix
A	Section area of the cable
C_m	Added mass coefficient
ζ_i	Damping ratio corresponding to the natural frequency of the structure
ω_i	Natural frequency of the structure
$\mathbf{F}_w^e$	Weight force
$\mathbf{F}_h^e$	Buoyancy force
$\mathbf{F}_d^e$	Drag force related to currents
$\mathbf{F}_f^e$	Force due to the seabed interaction
$\mathbf{F}_o^e$	Drag force due to waves
ρ_c	Cable density
ρ_a	Water density
D	Characteristic diameter of the element
C_{Dt}	Normal drag coefficient
C_{Dn}	Tangential drag coefficient
$\mathbf{U}_r^e$	Velocity relative to the element
dt	Time step
α	Parameter related with Bossak-Newmark implicit algorithm
γ, β	Parameters related to Newmark time integration scheme

9.2 Mooring system modelling

SeaFEM can handle complex mooring systems made up of various mooring lines attached to the floating structure. Each mooring line can be in turn composed of various segments each one resembling a chain, a steel cable or even a synthetic fiber. Forces resulting from the action of buoys and sinkers acting at the junctions between mooring line segments can also be considered. Hence, SeaFEM can deal with a wide variety of multi-segmented mooring line systems.

Cable tensions depend on the buoyancy and lateral displacements of the floating structure, the cable weight in water, the elasticity in the cable and the geometrical layout of the mooring system. Hence, as

the floating structure moves in response to unsteady environmental loadings, the mooring restraining forces change with the changing cable tension. This means that the mooring system has an effective compliance whose response is in general non-linear. Within SeaFEM, mooring inertia and damping are ignored, but the non-linear response is accounted for in the mooring system dynamics.

Mooring systems within SeaFEM are solved using a quasi-static approach in the sense that at any step of the calculation, and once the floating body displacements are known, the mooring system solver calculates the tensions and the geometrical configuration of each mooring line segment assuming that each cable is in static equilibrium at that instant. The mooring loads resulting from the calculation are added to the total load acting on the floating body, and the resulting dynamic equations of motion of the structure are solved again until convergence. At each time step the implicit non-linear system of equations describing the mooring system is solved using a classical Newton-Raphson scheme.

The formulation implemented within SeaFEM for dealing with catenary based mooring systems is outlined in what follows. Additionally, cables behaving as springs (both in tension and/or compression) can also be modeled.

9.2.1 Catenary equations

In a local coordinate system with its origin located at the lower cable point, the mooring equations for the catenary read as follows:

$$z = \left(\frac{T_o}{\omega}\right) cosh\left(\frac{\omega}{T_o}x + \alpha\right) + \beta \tag{9-1}$$

$$s = \left(\frac{T_o}{\omega}\right) sinh\left(\frac{\omega}{T_o}x + \alpha\right) + \gamma \tag{9-2}$$

where z is the vertical position, s is the catenary arc length, ω is the catenary weight per unit length in water, and T_o is the horizontal component of the cable tension which is constant everywhere. If the conditions $z(x = 0) = 0$ and $s(x = 0) = 0$ are applied, the equations result to be:

$$z = \left(\frac{T_o}{\omega}\right)\left[cosh\left(\frac{\omega}{T_o}x + \alpha\right) - \cosh(\alpha)\right] \tag{9-3}$$

$$s = \left(\frac{T_o}{\omega}\right)\left[sinh\left(\frac{\omega}{T_o}x + \alpha\right) - \sinh(\alpha)\right] \tag{9-4}$$

The action of any part of the line upon its neighbor is purely tangential, and the tangential direction can be written as:

$$tan\theta = \frac{dz}{dx} = \sinh\left(\frac{\omega}{T_o}x + \alpha\right) \tag{9-5}$$

The equilibrium equations can be written as:

$$\begin{aligned} &T_{down} \cdot cos\theta_{down} = T_{up} \cdot cos\theta_{up} = T_o \\ &T_{up} \cdot sin\theta_{up} - T_{down} \cdot sin\theta_{down} = \omega \cdot L \end{aligned} \tag{9-6}$$

From the horizontal component of the tension at any point of the catenary, it is possible to write the modulus of the cable tension at any point of the catenary as:

$$T = \frac{T_o}{cos\theta} = T_o \cdot \left(\sqrt{1 + tan^2\theta}\right) = T_o \cdot cosh\left(\frac{\omega}{T_o}x + \alpha\right) \tag{9-7}$$

Hence, the vertical component of tension at any point of the catenary can be written as:

$$T_v = T \cdot sin\theta = T_o \cdot sinh\left(\frac{\omega}{T_o}x + \alpha\right) \tag{9-8}$$

In particular, at the upper and bottom vertex of the catenary above equation reads, respectively:

$$T_{v\,up} = T_o \cdot sinh\left(\frac{\omega}{T_o}l + \alpha\right) \tag{9-9}$$

$$T_{v\,down} = T_o \cdot sinh(\alpha) \tag{9-10}$$

and the vertical equilibrium equation will result in:

$$L = \left(\frac{T_o}{\omega}\right)\left(sinh\left(\frac{\omega}{T_o}l + \alpha\right) - sinh\left(\alpha\right)\right) = s(x = l) \tag{9-11}$$

For a given length of the catenary (L) and for given horizontal and vertical distances (l, h) between the initial and end points of the catenary, it is possible to solve the equations by using a classical Newton-Raphson iterative process.

If the catenary has a seabed contact in its lower point, the following condition must be added

$$\left.\frac{dz}{dx}\right|_{x=0} = 0 \tag{9-12}$$

and the catenary equations result in:

$$\begin{aligned} z &= \left(\frac{T_o}{\omega}\right)\left[cosh\left(\frac{\omega}{T_o}x\right) - 1\right] \\ s &= \left(\frac{T_o}{\omega}\right)\left[sinh\left(\frac{\omega}{T_o}x\right)\right] \end{aligned} \tag{9-13}$$

9.2.2 Elastic catenary formulation

The elastic catenary formulation used within SeaFEM is similar to that presented in [6]. Each mooring line is analyzed in a local coordinate system that originates at the anchor. The local z-axis of this coordinate system is vertical and the local x-axis is directed horizontally from the anchor to the instantaneous position of the fairlead. When the mooring system module is called for a given structure displacement, SeaFEM first transforms each fairlead position from the global frame to this local system to determine its location relative to the anchor, x_F and z_F.

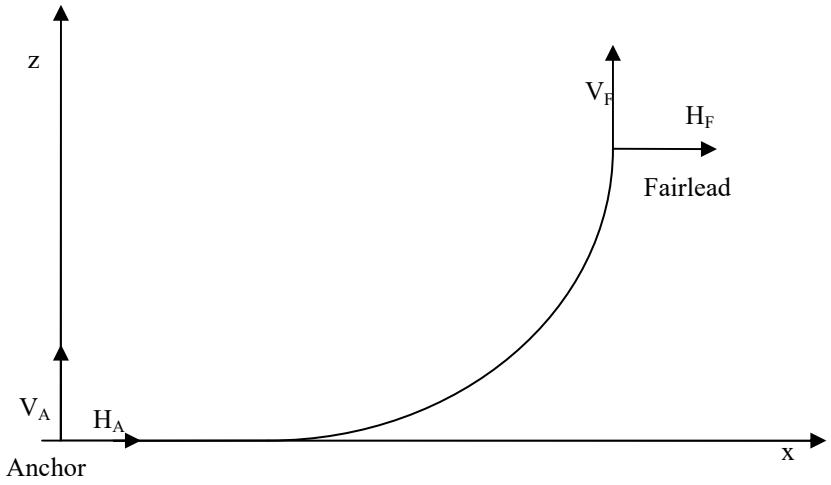

Figure 8: Catenary system of reference.

In the local coordinate system, the analytical formulation is given in terms of two nonlinear equations in two unknowns—the unknowns are the horizontal and vertical components of the effective tension in the mooring line at the fairlead, H_F and V_F, respectively.

$$z_F(H_F, V_F) = \frac{H_F}{\omega}\left[\sqrt{1+\left(\frac{V_F}{H_F}\right)^2} - \sqrt{1+\left(\frac{V_F-\omega L}{H_F}\right)^2}\right] + \frac{1}{EA}\left(V_F L - \frac{\omega L^2}{2}\right) \tag{9-14}$$

The analytical formulation of two equations in two unknowns is different when a portion of the mooring line adjacent to the anchor rests on the seabed:

$$\begin{aligned} x_F(H_F, V_F) &= L - \frac{V_F}{\omega} + \frac{H_F}{\omega} ln\left[\frac{V_F}{H_F} + \sqrt{1+\left(\frac{V_F}{H_F}\right)^2}\right] + \frac{H_F L}{EA} \\ &\quad + \frac{C_B \omega}{2EA}\left[-\left(L - \frac{V_F}{\omega}\right)^2 + \left(L - \frac{V_F}{\omega} - \frac{H_F}{C_B \omega}\right) MAX\left(L - \frac{V_F}{\omega} - \frac{H_F}{C_B \omega}, 0\right)\right] \\ z_F(H_F, V_F) &= \frac{H_F}{\omega}\left[\sqrt{1+\left(\frac{V_F}{H_F}\right)^2} - \sqrt{1+\left(\frac{V_F-\omega L_s}{H_F}\right)^2}\right] + \frac{1}{EA}\left(V_F L_s - \frac{\omega L_s^2}{2}\right) \\ L_B &= L - \frac{V_F}{\omega}, L_s = L - L_B \end{aligned} \tag{9-15}$$

The last term on the right-hand side of the x_F equation above, which involves C_B, corresponds to the stretched portion of the mooring line resting on the seabed that is affected by static friction. The seabed static friction was modeled simply as a drag force per unit length. The MAX function is needed to handle cases with and without tension at the anchor. Specifically, the resultant is zero when the anchor tension is positive; that is, the seabed friction is too weak to overcome the horizontal tension in the mooring line. Conversely, the resultant of the MAX function is nonzero when the anchor tension is zero. This happens when a section of cable lying on the seabed is long enough to ensure that the seabed friction entirely overcomes the horizontal tension in the mooring line. These equations consider that slack catenary is always tangent to the seabed at the point of touchdown.

The mooring system module uses a Newton-Raphson iteration scheme to solve nonlinear for the fairlead effective tension (H_F and V_F), given the line properties (L, ω, EA, and C_B) and the fairlead position relative to the anchor (x_F and z_F). The mooring system module uses the values of H_F and V_F from the previous time step as the initial guess in the next iteration of the Newton-Raphson scheme. As the model is being initialized, the following starting values, H_F^0 and V_F^0, are used [7]:

$$H_F^0 = \left|\frac{\omega x_F}{2\lambda_0}\right| \qquad V_F^0 = \frac{\omega}{2}\left[\frac{z_F}{tanh(\lambda_0)} + L\right] \tag{9-16}$$

where the dimensionless catenary parameter, λ_0, depends on the initial configuration of the mooring line:

$$\lambda_0 = \begin{cases} 1000000 & for\ x_F = 0 \\ 0.2 & for \sqrt{x_F^2 + z_F^2} \geq L \\ \sqrt{3\left(\frac{L^2 - z_F^2}{x_F^2} - 1\right)} & otherwise \end{cases} \tag{9-17}$$

Once the effective tension at the fairlead has been found, determining the horizontal and vertical components of the effective tension in the mooring line at the anchor, H_A and V_A, respectively, is simple. From a balance of external forces on a mooring line, one can easily verify that

$$H_A = H_F$$
$$V_A = V_F - \omega L \tag{9-18}$$

When no portion of the line rests on the seabed, and

$$H_A = MAX(H_F - C_B \omega L_B, 0)$$
$$V_A = 0 \tag{9-19}$$
$$L_B = L - \frac{V_F}{\omega}$$

The mooring system module solves the configuration of, and effective tensions within, the mooring line. When no portion of the mooring line rests on the seabed, the equations for the horizontal and vertical distances between the anchor and a given point on the line, x and z, and the equation for the effective tension in the line at that point, Te, are as follows:

$$x(s) = \frac{H_F}{\omega}\left\{ ln\left[\frac{V_A + \omega s}{H_F} + \sqrt{1 + \left(\frac{V_A + \omega s}{H_F}\right)^2}\right] - ln\left[\frac{V_A}{H_F} + \sqrt{1 + \left(\frac{V_A}{H_F}\right)^2}\right]\right\} + \frac{H_F s}{EA}$$
$$z(s) = \frac{H_F}{\omega}\left[\sqrt{1 + \left(\frac{V_A + \omega s}{H_F}\right)^2} - \sqrt{1 + \left(\frac{V_A}{H_F}\right)^2}\right] + \frac{1}{EA}\left(V_A s + \frac{\omega s^2}{2}\right) \tag{9-20}$$
$$T(s) = \sqrt{H_F^2 + (V_A + \omega s)^2}$$

where *s* is the unstretched arc distance along the mooring line from the anchor to the given point.
The equations with seabed interaction are:

$$x(s) = \begin{cases} s \quad for\ 0 \le s \le L_B - \dfrac{H_F}{C_B\omega} \\ s + \dfrac{C_B\omega}{2EA}\left[\begin{array}{c} s^2 - 2\left(L_B - \dfrac{H_F}{C_B\omega}\right)s + \\ \left(L_B - \dfrac{H_F}{C_B\omega}\right) max\left(L_B - \dfrac{H_F}{C_B\omega}, 0\right) \end{array}\right] \quad for\ L_B - \dfrac{H_F}{C_B\omega} \le s \le L_B \\ L_B + \dfrac{H_F}{\omega} ln\left[\dfrac{\omega(s-L_B)}{H_F} + \sqrt{1 + \left(\dfrac{\omega(s-L_B)}{H_F}\right)^2}\right] + \dfrac{H_F L}{EA} \quad for\ L_B \le s \le L \\ + \dfrac{C_B\omega}{2EA}\left[-(L_B)^2 + \left(L_B - \dfrac{H_F}{C_B\omega}\right) max\left(L_B - \dfrac{H_F}{C_B\omega}, 0\right)\right] \end{cases} \tag{9-21}$$

$$z(s) = \begin{cases} 0 \quad for\ 0 \le s \le L_B \\ \dfrac{H_F}{\omega}\left[\sqrt{1 + \left(\dfrac{\omega(s-L_B)}{H_F}\right)^2} - 1\right] + \dfrac{\omega(s-L_B)^2}{2EA} \quad for\ L_B \le s \le L \end{cases}$$

$$T(s) = \begin{cases} MAX(H_F + C_B\omega(s-L_B), 0) \\ \sqrt{H_F^2 + \left(\omega(s-L_B)\right)^2} \quad for\ L_B \le s \le L \end{cases}$$

The final calculation is a computation of the total load on the system from the contribution of all mooring lines. This mooring system-restoring load is found by first transforming each fairlead tension from its local mooring line coordinate system to the global frame, then summing up the tensions from all lines.

9.2.3 Dynamic cable formulation

SeaFEM includes a finite element model (FEM) for solving mooring line dynamics. For this purpose, the line is divided into a series of straight segments modeled by nonlinear truss elements, with three translational degrees of freedom per node. Lagrangian formulation is used to describe the dynamics of the mooring line.

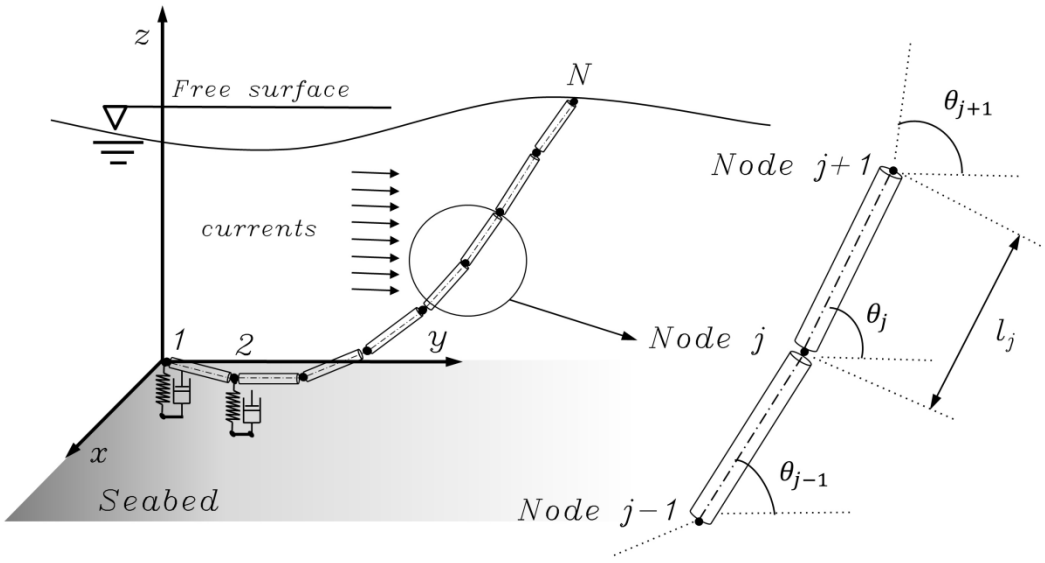

Figure 9: Scheme of the FEM cable model.

Applying FEM formulation to this nonlinear elastodynamics problem, the equations of the dynamics of the line can be written as follows:

$$\left(\overline{\overline{\mathbf{M}}}^{t+dt} + \overline{\overline{\mathbf{M}}}_A^{t+dt}\right)\ddot{\mathbf{x}} + \overline{\overline{\mathbf{C}}}^{t+dt}\dot{\mathbf{x}} + \mathbf{P}^0 + \mathbf{R}^{t+dt} = \mathbf{F}^{t+dt} \tag{9-22}$$

where x is the vector of nodal translational degrees of freedom, $\mathbf{F}$ the vector of external loads, $\overline{\overline{\mathbf{M}}}$ the inertia matrix of the line, $\overline{\overline{\mathbf{M}}}_A$ the added mass matrix, $\mathbf{P}^0$ is the pretension vector in the initial configuration, and $\mathbf{R}$, the vector of internal forces of the cable. Damping effects of mooring cable can be inserted through a Rayleigh-type damping matrix $\overline{\overline{\boldsymbol{C}}}$.

Considering the standard linearization of the internal forces, above equations can be expressed as:

$$\left(\overline{\overline{\mathbf{M}}}^{t+dt} + \overline{\overline{\mathbf{M}}}_A^{t+dt}\right)\ddot{\mathbf{x}} + \overline{\overline{\mathbf{C}}}^{t+dt}\dot{\mathbf{x}} + \mathbf{P}^0 + \left(\overline{\overline{\mathbf{K}}}^{t+dt} + \overline{\overline{\mathbf{K}}}_G^{t+dt}\right)\boldsymbol{\delta}\mathbf{x} + \mathbf{R}^t = \mathbf{F}^{t+dt} \tag{9-23}$$

where $\overline{\overline{\mathbf{K}}}$ and $\overline{\overline{\mathbf{K}}}_G$ are the so called material stiffness matrix and geometric stiffness matrix, respectively [7]. The corresponding elemental material stiffness matrix $\bar{\bar{\mathbf{k}}}^e$, and geometric stiffness matrix, $\bar{\bar{\mathbf{k}}}_G^e$, can be obtained in terms of the strain of the truss element, e:

$$\bar{\bar{\mathbf{k}}}^{e} + \bar{\bar{\mathbf{k}}}_{G}^{e} = \frac{\partial}{\partial x}\left(V^{e} s \frac{\partial e}{\partial x}\right) = V^{e} E \frac{\partial e}{\partial x} \otimes \frac{\partial e}{\partial x} + V^{e} s \frac{\partial^{2} e}{\partial x^{2}} \tag{9-24}$$

where V^{e} is the volume of the element, s the axial stress and E the axial elastic modulus. The FEM allows calculating those matrixes as follows [8]

$$\begin{aligned} \bar{\bar{\mathbf{k}}}^{e} &= V^{e} E \frac{\partial e}{\partial x} \otimes \frac{\partial e}{\partial x} = \int_{0}^{le} B_{o}^{T} V^{e} E B_{o} ds \\ \bar{\bar{\mathbf{k}}}_{G}^{e} &= V^{e} f \frac{\partial^{2} e}{\partial x^{2}} = \int_{0}^{le} B_{l}^{T} S B_{l}\, ds \end{aligned} \tag{9-25}$$

The elemental inertia matrixes are evaluated as:

$$\bar{\bar{\mathbf{m}}}^{e} = \int_{0}^{le} \bar{\bar{\mathbf{N}}}^{T} \rho \bar{\bar{\mathbf{N}}} ds \tag{9-26}$$

and the added mass matrix is calculated as

$$m_{a}{}^{e} = \rho A C_{m} \int_{0}^{le} \bar{\bar{\mathbf{N}}}^{T} \bar{\bar{\mathbf{N}}}\, ds \tag{9-27}$$

In the above equations, $\bar{\bar{\mathbf{N}}}$ is the general matrix of shape functions [8], A is the section area of the cable, and C_{m} is the added mass coefficient. Finally, the damping matrix is evaluated using the Rayleigh formulation:

$$\bar{\bar{\mathbf{C}}} = a_{1} \bar{\bar{\mathbf{K}}} + a_{2} \bar{\bar{\mathbf{M}}} \tag{9-28}$$

The coefficients a_{1}, a_{2} can be calculated as:

$$\zeta_{i} = \frac{1}{2}\left(\frac{a_{1}}{\omega_{i}} + a_{2} \omega_{i}\right) \tag{9-29}$$

where ζ_i is the damping ratio corresponding to the natural frequency ω_i of the structure. The external forces vector is evaluated by assembling the contribution of the different forces acting on the element:

$$\mathbf{F}^e = \mathbf{F}_w^e + \mathbf{F}_h^e + \mathbf{F}_d^e + \mathbf{F}_f^e + \mathbf{F}_o^e \tag{9-30}$$

where $\mathbf{F}_w^e$ is the weight, $\mathbf{F}_h^e$ is the buoyancy force, $\mathbf{F}_d^e$ is the drag force related to the currents, $\mathbf{F}_f^e$ is the force due to the seabed interaction and $\mathbf{F}_o^e$ is the drag force due to the waves. The weight and buoyancy force are calculated as follows

$$\begin{aligned} &\mathbf{F}_w^e + \mathbf{F}_h^e = \int_0^{le} f_{wh}^e \bar{\bar{\mathbf{N}}}\, ds, \\ &f_{wh}^e = f_w + f_h = g\frac{w(\rho_c - \rho_a)}{(1+e)\rho_c} \end{aligned} \tag{9-31}$$

where ρ_c is the density of the cable, ρ_a is the water density, w weight per meter and e the strain of the considered element. On the other hand, the drag force acting on the element, is evaluated as

$$\begin{aligned} &\mathbf{F}_d^e + \mathbf{F}_o^e = \int_0^{le} f_d^e \bar{\bar{\mathbf{N}}}\, ds, \\ &f_d^e = \int_0^{le} \frac{1}{2}\rho C_{Dt}\, D|U_r^e|U_r^e\, ds + \int_0^{le} \frac{1}{2}\rho C_{Dn}\, D|U_r^e|U_r^e\, ds \end{aligned} \tag{9-32}$$

where D is the characteristic diameter of the element, C_{Dt} and C_{Dn} the normal and tangential drag coefficients and U_r^e is the velocity relative to the element. The seabed interaction is modeled with the spring and normal and tangential damping terms given by:

$$\mathbf{F}_f^e = \int_0^{le} f_{ms}^e \bar{\bar{\mathbf{N}}}\, ds + \int_0^{le} f_{dn}^e \bar{\bar{\mathbf{N}}}\, ds + \int_0^{le} f_{dt}^e \bar{\bar{\mathbf{N}}}\, ds \tag{9-33}$$

where the vertical forces per unit length, due to the stiffness of the seabed f_{ms}^e, are expressed as

$$f_{ms}^{e} = \begin{cases} f_l wl & , \text{if } K_f\left[z_r - (z^e)^{t+dt}\right] \leq f_l wl \\ K_f\left[z_r - (z^e)^{t+dt}\right] & , \text{if } K_f\left[z_r - (z^e)^{t+dt}\right] > f_l wl \end{cases} \tag{9-34}$$

where z^e is the vertical coordinate of the corresponding node, l is the length of the cable associated to the node, and f_l is a coefficient of the model. K_f is the coefficient of the seabed normal stiffness force which has the magnitude:

$$K_f = G_k D l \tag{9-35}$$

where D is the diameter of the line, and G_k is the ground normal stiffness per unit length. The term z_r is then evaluated as:

$$z_r = z_i + \frac{wl}{G_k D} \tag{9-36}$$

The seabed damping forces are applied in the normal and tangential directions. The normal damping force is only applied when the penetrating object is travelling into the seabed. It is applied in the seabed outwards direction and has a magnitude given by:

$$f_{dn}^{e} = \begin{cases} D_n \dot{z}^e & , \text{if } \dot{z}^e < 0 \\ 0 & , \text{if } \dot{z}^e \geq 0 \end{cases} \tag{9-37}$$

and D_n is formulated as a fraction, G_c, of the critical damping

$$D_n = 2{,}0\, G_c \sqrt{G_k \left(\frac{wl^e}{g}\right)(Dl^e)} \tag{9-38}$$

Finally, the tangential damping force is again evaluated as a fraction, G_u, of the critical damping, and is applied in the direction opposing the tangential component of the velocity of the penetrator:

$$f_{dt}^{e} = D_t \dot{x}^e \tag{9-39}$$

$$D_t = 2{,}0\ G_c \sqrt{G_k \left(\frac{wl^e}{g}\right)(Dl^e)}$$

An implicit time integration scheme based on called Bossak-Newmark method [2] is applied to solve the system. It will lead to a system of algebraic equations to be solved in iterative manner:

$$\begin{aligned}\left[(1-\alpha)\left(\bar{\bar{\mathbf{M}}}^{t+dt,i} + \bar{\bar{\mathbf{M}}}_A^{t+dt,i}\right) + dt\gamma\bar{\bar{\mathbf{C}}}^{t+dt,i} + dt^2\beta\left(\bar{\bar{\mathbf{K}}}^{t+dt,i} + \bar{\bar{\mathbf{K}}}_G^{t+dt,i}\right)\right]\ddot{\mathbf{x}}^{t+dt,i+1} \\ = dt^2\beta\left(\bar{\bar{\mathbf{K}}}^{t+dt,i} + \bar{\bar{\mathbf{K}}}_G^{t+dt,i}\right)\ddot{\mathbf{x}}^{t+dt,i} + \mathbf{F}^{t+dt,i} - \mathbf{P}^0 + \mathbf{R}^t - \bar{\bar{\mathbf{C}}}^{t+dt,i}[\dot{\mathbf{x}}^t - dt(\gamma+1)\ddot{\mathbf{x}}^t] \\ - \alpha\left(\bar{\bar{\mathbf{M}}}^{t+dt,i} + \bar{\bar{\mathbf{M}}}_A^{t+dt,i}\right)\ddot{\mathbf{x}}^t\end{aligned} \quad (9\text{-}40)$$

where dt is time step, i denotes iteration, α is a parameter related with Bossak-Newmark implicit method, and γ and β are parameters related to Newmark time integration scheme. Finally, the new position and velocity of each node can be evaluated as:

$$\begin{aligned}\mathbf{x}^{t+\Delta t} &= \mathbf{x}^t + dt\,\dot{\mathbf{x}}^t + \frac{dt^2}{2}\left[(1-2\beta)\,\ddot{\mathbf{x}}^t + 2\beta\,\ddot{\mathbf{x}}^{t+dt}\right] \\ \dot{\mathbf{x}}^{t+\Delta t} &= \dot{\mathbf{x}}^t + dt\left[(1-\gamma)\,\ddot{\mathbf{x}}^t + \gamma\,\ddot{\mathbf{x}}^{t+dt}\right]\end{aligned} \quad (9\text{-}41)$$

The dynamic cable solver is integrated within SeaFEM dynamic solver. The scheme of the dynamics solver is presented in the section 7. In order to accelerate the scheme, the mooring forces are linearized within the body dynamics group, by evaluating the stiffness matrix K_M of the line. A detailed description of the FEM cable model implemented in SeaFEM can be found in [9].

10. FORCES ON SLENDER ELEMENTS

10.1 Glossary

$\boldsymbol{l}$	Unit vector denoting the local orientation of a long slender structural element
$\mathbf{v}$	Relative fluid velocity vector
$\mathbf{a}$	Relative acceleration of the submerged body
$\mathbf{a}^{b}$	Acceleration vector of any point of the body
$\mathbf{a}^{w}$	Fluid acceleration of the incident wave
$\mathbf{F}$	Force per unit length on a slender cylindrical element
$\mathbf{F}_{M}$	Inertia force per unit length
$\mathbf{F}_{L}$	Lift force per unit length
$\mathbf{F}_{D}$	Drag force per unit length
$\mathbf{F}_{V}$	Linear drag force per unit length
$\mathbf{F}_{F}$	Friction force per unit length
D	Characteristic linear dimension (the diameter in the case of a cylinder)
S	Cross section area
C_{M}	Added mass coefficient
C_{D}	Non-linear drag coefficient
C_{V}	Linear drag coefficient
C_{F}	Friction coefficient
C_{L}	Lift coefficient

10.2 Forces on slender elements

When viscous effects may be advanced to have a significant effect on the dynamic behavior of an offshore structure, Morison's equation can be used to evaluate wave loads on slender elements of the structure [9, 10, 11]. In SeaFEM, force corrections due to viscous effects can be also taken into account by using the Morison's equation. For this purpose, an auxiliary framework structure, associated to a body must be defined. See the SeaFEM user manual for details on how to define the auxiliary framework structure elements using the Tcl interface of SeaFEM.

Based on the information provided by the user, SeaFEM evaluates Morison's forces per unit length acting on the framework structure. After integration along the different elements, the resultant forces are incorporated to the dynamic solver of the rigid body to which the idealized framework structure has been associated. It is useful to write the Morison's equation in a vectorial formulation that automatically takes into account the actual orientation of structural elements and force components.
Considering a segment of a long slender structural element submerged into water its local orientation is given by a unit vector

$$\mathbf{l} = l\mathbf{i} + m\mathbf{j} + n\mathbf{k} \tag{10-1}$$

being l, m, n the directional cosines and (**l**, **j**, **k**) the unit vectors of the global coordinate system. Similarly, the relative fluid velocity vector and the relative acceleration vector of the submerged body are given by:

$$\begin{aligned} \mathbf{v} &= v_x\mathbf{i} + v_y\mathbf{j} + v_z\mathbf{k} \\ \mathbf{a} &= \mathbf{a^w} - \mathbf{a^b} = a_x\mathbf{i} + a_y\mathbf{j} + a_z\mathbf{k} \end{aligned} \tag{10-2}$$

The relative fluid velocity vector and the relative acceleration vector are evaluated based on the undisturbed wave potential equations.
The force per unit length on a slender cylindrical element may be written as the sum of inertia, drag, friction and lift forces:

$$\mathbf{F} = \mathbf{F}_M + \mathbf{F}_D + \mathbf{F}_V + \mathbf{F}_F + \mathbf{F}_L \tag{10-3}$$

where the inertia force F_M is oriented along the acceleration vector component normal to the element member, and its magnitude is proportional to the acceleration component. Lift force F_L is oriented normal to the velocity vector and normal to the axis of the element, and its magnitude is proportional the velocity squared. Drag force F_D is proportional to the squared velocity component normal to the element and normal to the lift force, while the linear drag force F_V is proportional to the velocity component normal to the element. Finally, friction force F_F is aligned along the axis of the element and proportional

to the squared velocity components tangential to the element axis. All these are satisfied if the various force components are defined as follows:

$$\mathbf{F}_M = (1-\delta_v)(1+C_M)\rho S(\mathbf{l}\times\mathbf{a}^{\mathbf{w}}\times\mathbf{l}) - \rho S C_M\left(\mathbf{l}\times\mathbf{a}^{\mathbf{b}}\times\mathbf{l}\right)$$
$$\mathbf{F}_D = \frac{1}{2}C_D\rho D|\mathbf{l}\times\mathbf{v}\times\mathbf{l}|(\mathbf{l}\times\mathbf{v}\times\mathbf{l})$$
$$\mathbf{F}_V = \frac{1}{2}C_V\rho D(\mathbf{l}\times\mathbf{v}\times\mathbf{l}) \qquad (10\text{-}4)$$
$$\mathbf{F}_F = \frac{1}{2}C_F\rho\pi D|\mathbf{l}\cdot\mathbf{v}|(\mathbf{l}\cdot\mathbf{v})\cdot\mathbf{l}$$
$$\mathbf{F}_L = \frac{1}{2}C_L\rho D|\mathbf{l}\times\mathbf{v}|(\mathbf{l}\times\mathbf{v})$$

where D is a linear dimension (the diameter in the case of a cylinder), S is the cross section area, C_M is the added mass coefficient, C_D is the non-linear drag coefficient, C_V is the linear drag coefficient, C_F is the friction coefficient, C_L is the lift coefficient, and δ_v takes the value 1 for virtual elements and 0 otherwise.

Remark: The first term in the right hand side of the $\mathbf{F}_M$ equation, includes the Froude-Kriloff force (i.e. undisturbed wave pressure force) and the diffraction inertial force, while the second term represents the radiation inertial force.

Remark: Note that while C_M, C_D, C_F, C_L are non-dimensional coefficients, C_V has dimensions of velocity.

As stated above, Eqs. (10-1) - (10-4) can estimate the different components of the force per unit length on a long (slender) structural element. Therefore, they can be integrated along the element axis, to obtain the additional forces an moments acting on the centre of gravity of the associated body.

11. RESPONSE AMPLITUDE OPERATORS (RAOs)

11.1 Glossary

N^w	Number of waves involved in the white noise spectrum for RAOs analysis
T_{min}	Minimum period for RAOs analysis
T_{max}	Maximum period for RAOs analysis
Δf	Frequency increment of the analysis
f_n	Discrete frequencies of the analysis
Δt	Time step
T	Total calculation time

11.2 Response amplitude operators (RAOs)

RAOs are transfer functions of the relation between the wave exciting forces and ship movements, used to determine the effect that a sea state will have upon the motion of a ship through the water.Calculation of Response Amplitude Operators (RAOs) in SeaFEM is done by analyzing the time series response of the ship, using a discretized white noise spectrum. This spectrum is defined by a number $N^w = 2^{m-1}$ of waves of equal amplitude and periods varying between the maximum and minimum values defined by the user. The values of these N^w periods are selected to match the discrete Fourier transform of the output signal, given by:

$$X = \sum_{n=0}^{N^w-1} x_n \cdot e^{-i2\pi\Delta f^* n} \tag{11-1}$$

Given T_{min} and T_{max}, the minimum and maximum periods of the analysis, the frequency increment is:

$$\Delta f = (f_{max} - f_{min})/(N^w - 1) = \left(\frac{1}{T_{min}} - \frac{1}{T_{max}}\right)/(N^w - 1) \quad (11\text{-}2)$$

The well-known Fast Fourier Transform algorithms give a procedure to obtain an exact evaluation of the transfer functions defined above. This way, the time step and the total computing time are internally fixed to match the required sampling time and total sampling points. Then, the holding frequency Δf^* is evaluated as

$$\Delta f^* = \min(\Delta f, f_{min}) \quad (11\text{-}3)$$

And the discrete frequencies are:

$$f_n = n \cdot \Delta f \quad n = 0, 1, 2, \dots, N^w - 1 \quad (11\text{-}4)$$

The required sampling frequency defines the time step as:

$$\Delta t = \frac{1}{2\Delta f^* \cdot 2^m} \quad (11\text{-}5)$$

The required number of sampling points defines the total calculation time as:

$$T = \frac{1}{\Delta f^*} \quad (11\text{-}6)$$

12. SOLVER ACCELERATION

12.1 Introduction

Most of the computational effort of the proposed numerical algorithm is spent in solving the linear system resulting from the wave diffraction-radiation problem. Therefore, our main focused in order to reduce the computational time is speeding up the linear solver. To do so, two techniques, that can be used combined, have been analyzed: the use of deflated solver, and the use of parallel computing in graphic processing units.

12.2 Solver deflation

Deflation works by considering piecewise constant approximations on coarse sub-domains. These piecewise constant approximations are associated to the low frequencies eigenmodes of the solution, which are also the slow convergence modes [12,13]. Then, these slow modes can be quickly approximated by solving a smaller linear system of equations that can be incorporated to the traditional preconditioned iterative solvers in order to accelerate the convergence of the solution. Hence, the use of preconditioning technique is compatible with the use of preconditioners.

The first step is to divide the domain into a set of coarse sub-domains capable of capturing the slow modes. Several techniques have been developed for this purpose [14,15]. Some authors has proposed a technique based on using seed-points to start building the sub-domains, and sub-domains are created by associating nodes to their closer seeds [15]. This technique has the disadvantage of requiring prescribing the seeds.

The algorithm developed for SeaFEM [1] is based on level structure criteria, where nodes are associated to a central node based on the level structure rooted at this central node (concept from graph theory). A maximum level structure “L”, where L refers to the neighbouring level respect to the central node, is prescribed. Figure 10 shows a domain decomposition obtained using this level structure technique with level L=2. Ordered pair (sub-domain, level) is used to identify nodes and sub-domains they belong to, and their corresponding structure level. Notice that nodes will accept to belong to a new sub-domain, if

and only if its structure level in that sub-domain is lower than its level in its current sub-domain. The algorithm used to obtain such decomposition is presented step by step next:

Step 0:	Assigned level L+1 to all nodes
Step 1:	Start building sub-domain 0: offer level 0 to the first node of the mesh (root node for sub-domain 0). It will become node (sub-domain, level)=(0,0)
Step 2:	Identify neighbours of the root node (node (0,0)) and offer them level 1: nodes (0,1)
Step 3:	Identify neighbours of nodes (0,1), and offer them level 2: nodes (0,2)
Step 4:	The procedure is repeated until the prescribed level “L” is reached
Step 5:	The first node still with level L+1 (based on the numbering of the nodes) is used as root node for sub-domain 1, and it is given level 0, becoming the root node (1,0)
Step 6:	Identify neighbours of the root node (1,0) and offer them level 1: nodes (1,1) (Notice that some (0,L) nodes might become (1,1))
Step 7:	Identify neighbours of nodes (1,1), and offer them level 2: nodes (1,2). (Notice that some (0,L) or (0,L-1) nodes might become (1,2) if L>2 or L-1>2 respectively)
Step 8:	The procedure is repeated until the nodes (1,L) are identified
Step 9:	Repeat Steps 5-8 until there is no node with level L+1

This algorithm guarantees that any node cannot have a lower structure level respect to any other root node. And the higher the prescribed level, the lower the number of sub-domains created.

Although the previous algorithm provides good results, it can be improved by using it twice. In a first round, rather than using the prescribed level L, a structure level 2L is used instead. Then a first decomposition is found with a lower number of sub-domains and twice the maximum structure level. In a second round, the procedure is repeated with a maximum structure level L and using as root those nodes with higher levels. Figure 10 shows the sub-domain decomposition obtained using the two rounds technique. The first one shows the decomposition after the first round at level 2L, and the second shows the decomposition after the second round at level L starting of the first decomposition at level 2L. Notice that the level at the sub-domains boundaries is lower or equal than the prescribed level L, and always minimum respect to any central node (node of level zero).

The recommended number of sub-domains might depend on the specific case under study. Usually in the order of hundred is a recommended value. In our specific case, the matrix of the linear system to be

solved remains the same during the calculation, so that the sub-domain decompositions have to be carried out just once.

The deflated system has to be solved every iteration of the solver. However, since in our case study the linear system of equation to be solved remains the same along the simulation, so does the deflated matrix. The inverse of the deflated matrix can be calculated just in the first time step, and then be stored. Hence, the resolution of the deflated system within each iteration can be substituted by a matrix vector multiplication.

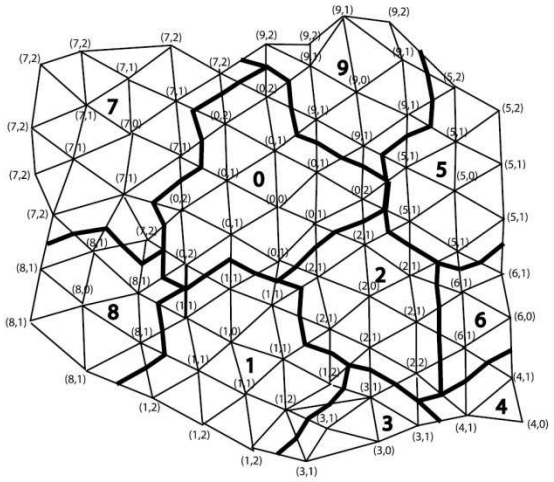

Figure 10: Sub-domain decomposition using the neighboring level algorithm

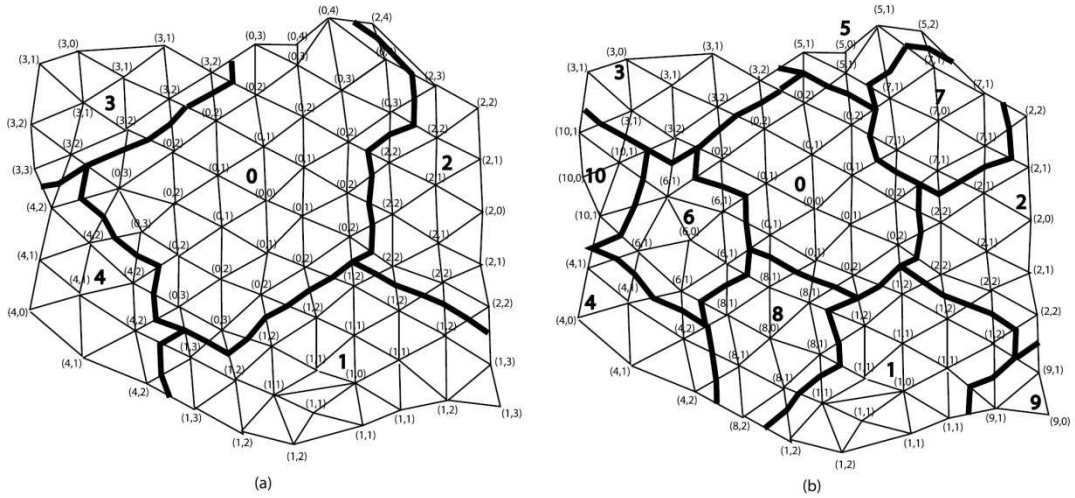

Figure 11: Sub-domain decomposition using the two-rounds neighboring level algorithm. (a) Decomposition after first round. (b) Decomposition after second round

12.3 Solver GPU acceleration

The fast development of the videogame industry is leading to higher computational capabilities of GPUs. Hence, their use for heavy computations in computational fluid dynamics is becoming more common (see [16,17]).

The implementation carried out in SeaFEM [1] is based on the well-known CUDA, a parallel computing platform and programming model invented by NVIDIA. It is focussed in speeding up the iterative solver using the functions provided by the cublas and cusparse libraries.

Deflated and non-deflated preconditioned conjugate gradient (CG) algorithm has been implemented in CUDA, along with a sparse approximate inverse (SPAI) preconditioner [18] and incomplete LU decomposition (ILU) preconditioner. However, using the sparse lower and upper triangular solvers provided in the cusparse library for ILU preconditioning resulted in poor performance. This poor performance can be expected since solving triangular system are not suitable for massive parallelization across tens of thousands threads [19], as required by GPUs in order to hide memory latency. Therefore we will omit the use of the ILU preconditioner when reporting GPU results.

Since the system matrix remains the same along the computation, preconditioners are calculated just once and in the first time step. Then, computational time invested in calculating preconditioners is negligible when compared to the total time spent in the linear solver during the whole simulation.

12.4 CPU Direct solver

SeaFEM has available a direct solver to be used with CPUs. It is advised to use this solver in those cases where the system matrix remains the same along the simulation. If the system matrix needs to be updated as the simulation advances, the direct solver will be slower when compared to iterative solvers.

12.5 OpenMP parallelization

OpenMP has been used for parallelization of CPU solvers as well as for evaluating analytical formulas. For instance, when evaluating irregular seas modelled by spectra discretization based on Airy waves, a large number of waves might be used, requiring a significant CPU time compared to the solver CPU time. Open MP has been used in SeaFEM to reduce the CPU time of this type of computations.

13. FLUID-STRUCTURE INTERACTION ALGORITHM

SeaFEM features a fluid-structure interaction algorithm, able to perform coupled analysis with the structural solver of the Tdyn's suite Ramseries.

The fluid-structure coupling is performed by an implicit iterative algorithm. This way, the pressure field computed in every iteration of the diffraction-radiation solver is sent to the structural solver to compute the body deformation. The resulting displacements are sent back to the fluid solver, and used as boundary condition to compute the new pressure field for the following iterations. The iterative process continues until the convergence norm condition is fulfilled; the relative distance of the pressure vectors between two successive iterations is below a given value. The iterative algorithm is accelerated using the Aitken method [6].

Since the diffraction-radiation and structural solvers are independent, the strategy used to communicate both solvers is based on the interchange of information at memory level by means of TCP-IP sockets. The library developed for this purpose, also takes care of the data interpolation from one mesh to another mesh.

14. MATHEMATICAL MODEL FOR FREQUENCY DOMAIN PROBLEMS

14.1 Glossary

Φ	Velocity potential
g	Gravity magnitude
A	Wave amplitude
ω	Circular frequency
K	Wave number
φ_0	Incident wave velocity potential
β	Angle between the direction of propagation of the incident wave and the positive x-axis
φ_R	Radiated component of the velocity potential
φ_D	Diffracted component of the velocity potential
ξ_j	Body's movement amplitude concerning ith degree of freedom
U	Body forward speed
ω_e	Encounter frequency
$A_{i,j}$	Added mass matrix
$B_{i,j}$	Damping matrix

14.2 Boundary element method

In SeaFEM, the Boundary Element Method (BEM) is used to solve problems stated within the framework of the frequency domain analysis. The frequency domain solver of SeaFEM is based on an adaptation of NEMOH, developed by Ecole Centrale de Nantes (for further information about NEMOH, see lheea.ec-nantes.fr/doku.php/emo/nemoh/start).

To solve the general equations, the boundary element method is used and applying Green's function, it allows taking into account the boundary conditions on body, bottom and free surface. BEM solver has

the following approach: it decouples the resolution of the linear free surface Boundary Value Problem and the definition of the boundary condition on the body.
Assuming an irrotational flow, the velocity can be expressed as the gradient of the velocity potential. The latter assumption along with incompressibility supposition leads to the Laplace equation:

$$\nabla^2\Phi = 0 \tag{14-1}$$

The first order dynamic free surface boundary condition is applied:

$$\Phi_t + g\varphi = 0 \tag{14-2}$$

And the kinematic free surface boundary condition establishes a relation between the free surface elevation φ and Φ:

$$\varphi_t = \Phi_z \tag{14-3}$$

Introducing (14-1) into (14-2), the equation becomes:

$$\Phi_{tt} + g\Phi_z = 0 \tag{14-4}$$

Assuming that the solution is of harmonic type, then the last equation becomes:

$$\Phi = \mathrm{Re}(Ae^{i\omega t}) \tag{14-5}$$

$$-\omega^2 \cdot \Phi + g\Phi_z = 0 \tag{14-6}$$

In the frequency domain, the first order free surface boundary condition becomes:

$$\Phi_z - \mathrm{K} \cdot \Phi = 0 \quad , \quad K = \omega^2/g \tag{14-7}$$

The velocity potential of the incident wave is defined as:

$$\varphi_0 = \frac{i \cdot g \cdot A}{\omega} \cdot \frac{\cosh[k \cdot (z+h)]}{\cosh k \cdot H} \cdot e^{-i \cdot k \cdot x \cdot \cos\beta - i \cdot k \cdot y \cdot \sin\beta} \quad (14\text{-}8)$$

Where k fulfils dispersion relation:

$$\frac{\omega^2}{g} = k \cdot \tanh k \cdot H \quad (14\text{-}9)$$

And β is the angle between the direction of propagation of the incident wave and the positive x-axis.

As the problem is linearized, the velocity potential can be decomposed into two components: radiation and diffraction.

$$\varphi = \varphi_R + \varphi_D \quad (14\text{-}10)$$

$$\varphi_R = i \cdot \omega \cdot \sum_{j=1}^{6} \xi_j \cdot \varphi_j \quad (14\text{-}11)$$

$$\varphi_D = \varphi_0 + \varphi_S \quad (14\text{-}12)$$

Where ξ_j denotes the amplitude of the body's movement in its six degrees of freedom and φ_j the corresponding unit-amplitude radiation potentials.

14.3 Forward speed corrections

Assuming a forward speed of the bodies as $velocity = U, direction = \beta$, then a few corrections have to be made to take into account this effect. First, the frequency has to be changed to a frequency of wave encounter:

$$\omega_e = \omega - k \cdot U \cdot \cos\beta \quad (14\text{-}13)$$

Here k is the wave number, ω the frequency without velocity and ω_e the encounter frequency. Other changes to be made are for the added mass and damping matrixes:

$$A_{3,5} = -\frac{U}{\omega^2} \cdot B^0_{3,3} \tag{14-14}$$

$$B_{3,5} = +U \cdot A^0_{3,3} \tag{14-15}$$

$$A_{5,3} = +\frac{U}{\omega^2} \cdot B^0_{3,3} \tag{14-16}$$

$$A_{5,3} = +\frac{U}{\omega^2} \cdot B^0_{3,3} \tag{14-17}$$

$$B_{5,5} = +\frac{U^2}{\omega^2} \cdot A^0_{3,3} \tag{14-18}$$

This formulation has been taken from the one presented in [19].

REFERENCES

[1] Serván-Camas, B., and García-Espinosa, J. Accelerated 3D multi-body seakeeping simulations using unstructured finite elements. Journal of Computational Physics 252 (2013) 382–403.

[2] Wood W. L., Bossak M., and Zienkiewicz O. C. An alpha modication of Newmark's method. International Journal for Numerical Methods in Engineering, 1980, 15(10):1562-1566.

[3] Pierson J.P. and Moskowitz L. A Proposed Spectral Form for Fully Developed Wind Seas Based on the Similarity Theory of S.A.Kitaigorodskii. Journal of Geophysical Research, 1964, Vol. 69, No.24.

[4] Faltinsen O.M., Sea loads on ships and offshore structures, Cambridge Ocean Technology Series. 1998.

[5] Hasselmann K., Barnett R.C., Bouws E., Carlson H., Cartwright D.E., Enke K., Ewing J.A., Gienapp H., Hasselmann D.E., Kruseman P., Meerburg A., Müller P., Olbers, D.J., Richter K., Sell W., Walden H. Measurements of Wind-Wave Growth and Swell Decay during the Joint North Sea Wave Project (JONSWAP). Deutches Hydrographisches Institut, 1973, No.12.

[6] Jonkman, J.M., Dynamic modelling and loads analysis of an offshore floating wind turbine, Technical report NREL/TP-500-41958; November 2007.

[7] Bathe, K.H. Finite element procedures. Prentice Hall, 1996.

[8] Gutiérrez, J.E. Desarrollo de herramientas software para el análisis de aerogeneradores “offshore” sometidos a cargas acopladas de viento y oleaje. PhD dissertation, Universidad Politécnica de Cartagena (2014).

[9] Morison J. R., O’Brien M. P., Johnson J. W., and Schaaf S. A., 1950, The force exerted by surface waves on piles. Petroleum Transactions, American Institute of Mining Engineers, 189, pp. 149–154.

[10] Recommended practice DNV-RP-C205. Environmental conditions and environ-mental loads. April 2007.

[11] Det Norske Veritas. A Course in Ocean engineering. Available at: <http://research.dnv.com/hci/ocean/bk/c/a36/s0.htm>.

[12] Aubry, R., Mut, F., Löhner, R., Cebral, J.R.: Deflated preconditioned conjugate gradient solvers for the Pressure–Poisson equation, J. Comp. Phys. 2008; 227: 10196-10208.

[13] Mut, F., Aubry, R., Houzeaux, G., Cebral, J., Löhner, R.: Deflated preconditioned conjugate gradient solvers: extensions and improvements, 48th Aerospace Sciences Meeting and Exhibit, Orlando, FL, January, 2010.

[14] Aubry, R., Mut, F., Löhner, R., Cebral, J.R.: Deflated preconditioned conjugate gradient solvers for the Pressure–Poisson equation, J. Comp. Phys. 2008; 227: 10196-10208.

[15] Mut, F., Aubry, R., Houzeaux, G., Cebral, J., Löhner, R.: Deflated preconditioned conjugate gradient solvers: extensions and improvements, 48th Aerospace Sciences Meeting and Exhibit, Orlando, FL, January, 2010.

[16] Mossaiby, F., Rossi, R., Dadvand, P., Idelsohn, S.: OpenCL-based implementation of an unstructured edge-based finite element convection-diffusion solver on graphics hardware. Int. J. Numer. Meth. Engng. 2011; 89, 13: 1635–1651.

[17] Bell, N., Garland, M.: Effcient Sparse Matrix-Vector Multiplication on CUDA, NVIDIA Technical Report NVR-2008-004, Dec. 2008.

[18] Saad, Y.: Iterative Methods for Sparse Linear Systems. PWS Publishing Company, Boston (1996).

[19] Salvesen, N., Tuck, E.O. and Faltinsen, O.M. Ship Motions and Sea Loads, Trans. SNAME, 78, 250-87 (1970).

[20] Servan-Camas, B.: A time-domain finite element method for seakeeping and wave resistance problems. School of Naval Architecture and OCean Engineering, Technical University of Madrid; 2016 [Doctoral thesis]. http://oa.upm.es/39794/1/BORJA_SERVAN_CAMAS.pdf